Cytochrome *c* Oxidase Models: A Dinuclear Iron(III) Porphyrin–Copper(II) Complex with a Sulfur Bridge

Barbara R. Serr,[†] Christine E. L. Headford,[†] Oren P. Anderson,*[,†] C. Michael Elliott,*[,†] Kevork Spartalian,[‡] Vladimir E. Fainzilberg,[⊥] William E. Hatfield,[§] Brian R. Rohrs,[§] Sandra S. Eaton,[∥] and Gareth R. Eaton[∥]

Department of Chemistry, Colorado State University, Fort Collins, Colorado 80523, Department of Physics, University of Vermont, Burlington, Vermont 05405, Department of Chemistry, The University of North Carolina, Chapel Hill, North Carolina 27599, and Department of Chemistry, University of Denver, Denver, Colorado 80208, Department of Chemistry, Long Island University, Brookville, New York 11548

Received October 12, 1990

Three compounds, each containing a dinuclear anion in which an iron(III) porphyrin and a copper(II) atom are bridged by a sulfur atom, have been synthesized and characterized: $[Fe(TPP)(THF)_2]\{[Fe(TPP)(THF)][Cu(MNT)_2]\}\cdot 2THF$ (**1**), $[Ga(TPP)(THF)_2]\{[Fe(TPP)(THF)][Cu(MNT)_2]\}\cdot 2THF$ (**2**), and $[Al(TPP)(THF)(OH_2)]\{[Fe(TPP)(THF)][Cu(MNT)_2]\}\cdot 3THF$ (**3**) (TPP^{2-} = 5,10,15,20-tetraphenylporphyrinate, THF = tetrahydrofuran, MNT^{2-} = *cis*-1,2-dicyanoethylenedithiolate). The structures of **1** (triclinic, $Z = 1$, space group $P\bar{1}$; at 20 °C, a = 11.622 (2) Å, b = 13.592 (2) Å, c = 16.696 (2) Å, α = 83.60 (1)°, β = 74.91 (1)°, γ = 88.60 (1)°; at −130 °C, a = 11.463 (3) Å, b = 13.351 (3) Å, c = 16.643 (4) Å, α = 82.37 (2)°, β = 74.07 (2)°, γ = 89.28 (2)°), of **2** (triclinic, $Z = 1$, space group $P\bar{1}$; at −130 °C, a = 11.478 (4) Å, b = 13.375 (4) Å, c = 16.665 (5) Å, α = 82.08 (2)°, β = 73.93 (2)°, γ = 89.19 (2)°), and of **3** (triclinic, $Z = 1$, space group $P\bar{1}$; at −60 °C, a = 11.511 (2) Å, b = 13.489 (3) Å, c = 16.481 (3) Å, α = 84.19 (1)°, β = 75.22 (1)°, γ = 89.09 (2)°) have been determined by single-crystal X-ray diffraction. The dinuclear anion in each compound consists of an iron(III) porphyrin that is bound to a $[Cu(MNT)_2]^{2-}$ anion by coordination of one of the sulfur atoms of the copper(II) complex at an axial position; in each case, the sixth coordination site about the iron atom is occupied by a THF molecule. The structural results and the Mössbauer parameters suggest intermediate spin-state assignments for the iron(III) atoms of the dinuclear anions in each compound. The exchange coupling constants calculated from the magnetic susceptibility data (J = −17.94 cm^{-1} for **2**, −15.18 cm^{-1} for **3**) demonstrate the existence of weak antiferromagnetic coupling between the iron and copper metal centers in these dinuclear anions. The dinuclear anion in **1**–**3** does not exhibit an EPR spectrum at 5 K and 9.5 GHz. The absence of EPR signals for **2** and **3** is consistent with calculations that show that the values of J and D for these complexes are sufficiently large that the energies required for allowed transitions are greater than the X-band EPR quantum at the magnetic fields used to obtain the experimental data.

Introduction

Cytochrome *c* oxidase (CcO) catalyzes the reduction of O_2 to H_2O. Four redox-active metal centers (Fe_a, Cu_A, Fe_{a3}, and Cu_B) participate in this reduction, in which O_2 is believed to bind to the Fe_{a3} heme in close proximity to Cu_B.[1] The origin of the unusual magnetic and spectroscopic properties exhibited by the resting oxidized form of the enzyme remains a matter of much interest. In particular, the reason for the absence of an EPR signal from the Fe_{a3}–Cu_B site has been the subject of considerable speculation. The most widely accepted explanation for this EPR silence invokes strong ligand-mediated antiferromagnetic coupling ($-J > 200$ cm^{-1}) between the Cu(II) and Fe(III) centers.[2] Another possible explanation[3] invokes ligand-mediated spin-relaxation broadening between these metals; this explanation does not require that the degree of exchange coupling between the metal centers be large.

A variety of complexes have been synthesized as models for the active site of the resting oxidized form of the enzyme. These complexes have employed various bridging ligands, including imidazolate,[4] oxygen,[5] halogens or pseudohalogens,[6] and bipyrimidyl.[7] None of these model complexes has exhibited antiferromagnetic coupling between the metal centers as large as $-J > 200$ cm^{-1}.

We have previously characterized trinuclear complexes involving iron(III) porphyrins and copper(II) complexes in which sulfur atoms link the two metals.[3,8] Systems in which sulfur was

* Authors to whom correspondence should be addressed.
† Colorado State University.
‡ University of Vermont.
§ The University of North Carolina.
∥ University of Denver
⊥ Long Island University.

(1) Malmström, B. G. In *Metal Ion Activation of Dioxygen*; Spiro, T. G., Ed.; Wiley: New York, 1980; Chapter 5.
(2) Palmer, G.; Babcock, G. T.; Vickery, L. E. *Proc. Natl. Acad. Sci. U.S.A.* **1976**, *73*, 2206.
(3) Elliott, C. M.; Akabori, K. *J. Am. Chem. Soc.* **1982**, *104*, 2671.
(4) (a) Dessens, S. E.; Merill, C. L.; Saxton, R. J.; Ilaria, R. L.; Lindsey, J. W.; Wilson, L. J. *J. Am. Chem. Soc.* **1982**, *104*, 4357. (b) Wilson, L. J.; Chunplang, V.; Lemke, B. K.; Merrill, C. L.; Saxton, R. J.; Watson, M. L. *Inorg. Chim. Acta* **1983**, *79*, 107. (c) Saxton, R. J.; Wilson, L. J. *J. Chem. Soc., Chem. Commun.* **1984**, 359. (d) Cutler, A. C.; Brittain, T.; Boyd, P. D. W. *J. Inorg. Biochem.* **1985**, *24*, 199. (e) Chunplang, V.; Wilson, L. J. *J. Chem. Soc., Chem. Commun.* **1985**, 1761. (f) Brewer, C. T.; Brewer, G. *J. Inorg. Biochem.* **1986**, *26*, 247. (g) Brewer, C. T.; Brewer, G. A. *Inorg. Chem.* **1987**, *26*, 3420.
(5) (a) Gunter, M. J.; Mander, L. N.; Murray, K. S. *J. Chem. Soc., Chem. Commun.* **1981**, 799. (b) Gunter, M. J.; Mander, L. N.; Murray, K. S.; Clark, P. E. *J. Am. Chem. Soc.* **1981**, *103*, 6784. (c) Chang, C. K.; Koo, M. S.; Ward, B. *J. Chem. Soc., Chem. Commun.* **1982**, 716. (d) Lukas, B.; Miller, J. R.; Silver, J.; Wilson, M. T.; Morrison, I. E. G. *J. Chem. Soc., Dalton Trans.* **1982**, 1035. (e) Saxton, R. J.; Olson, L. W.; Wilson, L. J. *J. Chem. Soc., Chem. Commun.* **1982**, 984. (f) Journaux, Y.; Kahn, O.; Zarembowitch, J.; Galy, J.; Jaud, J. *J. Am. Chem. Soc.* **1983**, *105*, 7585. (g) Kanda, W.; Okawa, H.; Kida, S. *Bull. Chem. Soc. Jpn.* **1984**, *57*, 1159. (h) Elliott, C. M.; Jain, N. C.; Cranmer, B. K.; Hamburg, A. W. *Inorg. Chem.* **1987**, *26*, 3655.

0020-1669/92/1331-5450$03.00/0

Table I. Crystallographic Parameters and Refinement Results

	compd			
	1	**1**	**2**	**3**
mol formula	$C_{116}H_{96}N_{12}CuFe_2O_5S_4$	$C_{116}H_{96}N_{12}CuFe_2O_5S_4$	$C_{116}H_{96}N_{12}CuFeGaO_5S_4$	$C_{116}H_{98}N_{12}AlCuFeO_6S_4$
mol weight	2041.7	2041.7	2055.6	2030.7
space group	*P*1	*P*1	*P*1	*P*1
temp, °C	20	−130	−130	−60
a, Å	11.622 (2)	11.463 (3)	11.478 (4)	11.511 (2)
b, Å	13.592 (2)	13.351 (3)	13.375 (4)	13.489 (3)
c, Å	16.696 (2)	16.643 (4)	16.665 (5)	16.481 (3)
α, deg	83.60 (1)	82.37 (2)	82.08 (2)	84.19 (1)
β, deg	74.91 (1)	74.07 (2)	73.93 (2)	75.22 (1)
γ, deg	88.60 (1)	89.28 (2)	89.19 (2)	89.09 (2)
V, Å^3	2530	2427	2434	2461
Z	1	1	1	1
D(calcd), g cm^{-3}	1.34	1.40	1.40	1.37
radiation	Mo Kα^a	Mo Kα^a	Mo Kα^a	Mo Kα^a
μ, cm^{-1}	6.3	6.6	8.0	5.2
R	0.109	0.085	0.095	0.100
R_w	0.117	0.091	0.101	0.108

^{a} λ = 0.7107 Å.

employed as a bridging atom were chosen for study on the basis of EXAFS studies on CcO, which have suggested the presence of a third-row ligand (S or Cl) about the Fe(III) and the Cu(II) of the presumed active site.[9,10] Herein, we discuss the characterization of three compounds, each of which contains an Fe(III)–S–Cu(II) unit in the dinuclear anion $\{[Fe(TPP)(THF)][Cu(MNT)_2]\}^-$. The synthesis and some of the properties of the first of these compounds, $[Fe(TPP)(THF)_2]\{[Fe(TPP)(THF)][Cu(MNT)_2]\}\cdot 2THF$ (hereafter **1**, TPP^{2-} = 5,10,15,20-tetraphenylporphyrinate, THF = tetrahydrofuran, MNT^{2-} = *cis*-1,2-dicyanoethylenedithiolate) were discussed in a preliminary report.[11] In that case, the presence of the paramagnetic $[Fe(TPP)(THF)_2]^+$ cation made unambiguous interpretation of the spectroscopic and magnetic properties of the coupled Fe(III)–S–Cu(II) system of the dinuclear anion difficult. Attempts to simplify the interpretation of the spectroscopic and magnetic properties by replacement of the paramagnetic $[Fe(TPP)(THF)_2]^+$ cation with diamagnetic cations of similar structure resulted in preparation of $[Ga(TPP)(THF)_2]\{[Fe(TPP)(THF)][Cu(MNT)_2]\}\cdot 2THF$ (hereafter **2**) and $[Al(TPP)(THF)(OH_2)]\{[Fe(TPP)(THF)][Cu(MNT)_2]\}\cdot 3THF$ (hereafter **3**) as described below.

Experimental Section

Materials. All solvents and reagents were purchased commercially and used as supplied except as follows. THF and *n*-hexane were distilled under N_2 from sodium benzophenone ketyl. Fe(TPP) was prepared and purified according to published procedures for other Fe(II) porphyrins.[12] $(TBA)[Cu(MNT)_2]$ (TBA^+ = tetra-*n*-butylammonium) was prepared by dichlorodicyanobenzoquinone oxidation of $(TBA)_2[Cu(MNT)_2]$[13] in CH_2Cl_2. $[Al(TPP)(OH_2)]Cl$ was prepared according to published procedures[14] and purified by chromatography on an alumina column with gradient elution by CH_2Cl_2, THF, and $CHCl_3$. $[Ga(TPP)](O_3SCF_3)$ and $[Al(TPP)(OH_2)](O_3SCF_3)$ were prepared by reaction of equimolar amounts of $[Ga(TPP)]Cl$[15] or $[Al(TPP)(OH_2)]Cl$ and AgO_3SCF_3 in THF.

Synthesis of $[Fe(TPP)(THF)_2]\{[Fe(TPP)(THF)][Cu(MNT)_2]\}\cdot 2THF$ (1). This compound was prepared in two ways.

(a) Fe(TPP) (0.054 g, 0.08 mmol) was dissolved in THF (60 mL) under N_2. Solid $(TBA)[Cu(MNT)_2]$ (0.047 g, 0.08 mmol) was added, and the reaction mixture was stirred at room temperature for 2.5 h. Vapor diffusion of *n*-hexane into the reaction solution over a period of 1–2 weeks yielded dark crystals of **1** (~70% yield).

(b) The trinuclear complex $\{[Fe(TPP)]_2[Cu(MNT)_2]\}$[3] was recrystallized from THF under N_2. In a typical case, $\{[Fe(TPP)]_2[Cu(MNT)_2]\}$ (0.100 g, 0.006 mmol) was dissolved in THF (100 mL); vapor diffusion of *n*-hexane into the solution over a period of 1–2 weeks yielded dark crystals of **1**.

Crystals of the products obtained by methods a and b exhibited unit cell constants that were identical within experimental error; visible spectra of the two products in *o*-dichlorobenzene were also identical.

Synthesis of $[Ga(TPP)(THF)_2]\{[Fe(TPP)(THF)][Cu(MNT)_2]\}\cdot 2THF$ (2). Fe(TPP) (0.08 mmol) was dissolved in THF (50 mL) under N_2. Solid $(TBA)[Cu(MNT)_2]$ (0.08 mmol) was added, and the reaction mixture was stirred at room temperature for 2 h. A solution of $[Ga(TPP)](O_3SCF_3)$ (0.08 mmol) in THF (30 mL) was added; vapor diffusion of *n*-hexane into the solution over a period of 1–2 weeks yielded dark crystals of **2**.

Synthesis of $[Al(TPP)(THF)(OH_2)]\{[Fe(TPP)(THF)][Cu(MNT)_2]\}\cdot 3THF$ (3). This complex was prepared in the same manner as **2**, except that a solution of $[Al(TPP)(OH_2)](O_3SCF_3)$ (0.08 mmol) in THF (30 mL) rather than $[Ga(TPP)](O_3SCF_3)$ was added prior to crystallization.

X-ray Structure Determinations. Crystal data for **1** (at 20 and −130 °C), **2**, and **3** are reported in Table I. Cell constants were obtained by least-squares refinement of the setting angles for 25 reflections ($2\theta_{av}$ = 27.12° (20 °C) and 27.81° (−130 °C) for **1**, 22.26° for **2**, and 21.56° for **3**) on a Nicolet R3m diffractometer.[16] The stability of the crystal of **1** used was monitored during data collection by measurement of the intensities of standard reflections ($\bar{2}00$, 020, 002 at 20 °C and 200, 020, 002 at −130 °C) every 197 data points, as were the stabilities of **2** and **3** (standard reflections 200, 020, 002 for both). Over the course of the data collections, no significant changes in the intensity of any of the standard reflections were noted. Lorentz and polarization corrections were applied in each case.

Crystals of **3** were found to crack upon cooling to −130 °C. By placing a crystal of **3** on the diffractometer, slowly lowering the temperature, and monitoring the stability of the crystal with rotation photos, we found that

(6) (a) Gunter, M. J.; Mander, L. N.; McLaughlin, G. M.; Murray, K. S.; Berry, K. J.; Clark, P. E.; Buckingham, D. A. *J. Am. Chem. Soc.* **1980**, *102*, 1470. (b) Berry, K. J.; Gunter, M. J.; Murray, K. S. *Nouv. J. Chim.* **1980**, *4*, 581. (c) Gunter, M. J.; Berry, K. J.; Murray, K. S. *J. Am. Chem. Soc.* **1984**, *106*, 4227.
(7) (a) Petty, R. H.; Welch, B. R.; Wilson, L. J.; Bottomly, L. A.; Kadish, K. M. *J. Am. Chem. Soc.* **1980**, *102*, 611. (b) Brewer, G. A.; Sinn, E. *Inorg. Chem.* **1984**, *23*, 2532.
(8) (a) Schauer, C. K.; Akabori, K.; Elliott, C. M.; Anderson, O. P. *J. Am. Chem. Soc.* **1984**, *106*, 1127. (b) Serr, B. R.; Headford, C. E. L.; Anderson, O. P.; Elliott, C. M.; Schauer, C. K.; Akabori, K.; Spartalian, K.; Hatfield, W. E.; Rohrs, B. R. *Inorg. Chem.* **1990**, *29*, 2663–2671.
(9) Powers, L.; Chance, B.; Ching, Y.; Angiolillo, P. *Biophys. J.* **1981**, *34*, 465.
(10) Li, P. M.; Gelles, J.; Chan, S. I.; Sullivan, R. J.; Scott, R. A. *Biochemistry* **1987**, *26*, 2091.
(11) Serr, B. R.; Headford, C. E. L.; Elliott, C. M.; Anderson, O. P. *J. Chem. Soc., Chem. Commun.* **1988**, 92.
(12) Collman, J. P.; Brauman, J. D.; Doxsee, K. M.; Halbert, T. R.; Bunnenbert, E.; Linder, R. E.; LaMar, G. N.; Grandio, J. D.; Lang, G.; Spartalian, K. *J. Am. Chem. Soc.* **1980**, *102*, 4182.
(13) Muetterties, E. L., Ed. *Inorganic Syntheses*; McGraw Hill: New York, 1961; Vol. X, p 13.
(14) Aida, T.; Mizuta, R.; Yoshida, Y.; Inoue, S. *Makromol. Chem.* **1981**, *182*, 1073.
(15) Supplied by Professor K. M. Kadish, University of Houston.

Table II. Atomic Coordinates ($\times 10^4$) and Isotropic Thermal Parameters ($Å^2 \times 10^3$)[a] for **1** at −130 °C

atom	x	y	z	U_{iso}[b]	atom	x	y	z	U_{iso}[b]
Fe1	0	0	0	12 (1)*	C60	−1394 (9)	−2249 (9)	870 (7)	29 (3)*
Fe2	4085 (1)	4501 (1)	4572 (1)	13 (1)*	C61	−2583 (10)	−1985 (8)	1379 (7)	34 (4)*
Cu	530 (1)	−2669 (1)	−761 (1)	28 (1)*	C62	−768 (9)	−2984 (8)	1162 (7)	29 (3)*
N1	−1139 (6)	61 (5)	1146 (4)	14 (2)*	C63	−1141 (12)	−3460 (9)	2011 (8)	42 (4)*
N2	1237 (7)	−611 (6)	557 (5)	17 (3)*	C64	2349 (9)	−3097 (7)	−2415 (7)	22 (3)*
N3	1186 (6)	39 (5)	−1126 (4)	15 (2)*	C65	3492 (10)	−3353 (8)	−2986 (7)	29 (4)*
N4	−1188 (6)	707 (5)	−541 (4)	12 (2)*	C66	1631 (9)	−2364 (8)	−2662 (6)	24 (3)*
N5	2782 (7)	5061 (6)	4017 (5)	18 (3)*	C67	2010 (9)	−1822 (7)	−3511 (7)	25 (3)*
N6	2880 (6)	4524 (5)	5728 (4)	13 (2)*	C71	1676 (8)	5388 (7)	4402 (5)	16 (3)*
N7	5330 (7)	3875 (6)	5145 (5)	20 (3)*	C72	1119 (7)	5899 (6)	3803 (5)	15 (2)*
N8	5289 (6)	4464 (5)	3422 (5)	16 (2)*	C73	1946 (8)	5881 (7)	3009 (6)	20 (3)*
N9	−3512 (10)	−1779 (8)	1791 (10)	67 (5)*	C74	2968 (8)	5346 (7)	3154 (5)	17 (3)*
N10	−1461 (12)	−3797 (7)	2725 (6)	50 (4)*	C75	4026 (7)	5243 (6)	2535 (5)	14 (3)*
N11	4311 (11)	−3528 (8)	−3389 (6)	49 (4)*	C76	5068 (8)	4774 (7)	2668 (5)	19 (3)*
N12	2225 (7)	−1465 (8)	−4145 (5)	33 (3)*	C77	6125 (8)	4564 (7)	1996 (6)	19 (3)*
S1	−898 (3)	−1563 (2)	−149 (2)	34 (1)	C78	6936 (9)	4105 (7)	2369 (6)	22 (2)*
S2	546 (3)	−3423 (3)	539 (2)	44 (1)*	C79	6404 (8)	4040 (6)	3268 (5)	15 (2)*
S3	2012 (2)	−3666 (2)	−1372 (2)	28 (1)*	C80	6983 (8)	3609 (7)	3879 (6)	20 (3)*
S4	305 (3)	−1986 (2)	−2009 (2)	30 (1)*	C81	6473 (7)	3557 (6)	4739 (5)	13 (3)*
O1	614 (6)	1535 (5)	92 (4)	24 (2)*	C82	7048 (9)	3109 (7)	5384 (6)	24 (3)*
O2	4701 (7)	6018 (5)	4533 (5)	35 (3)*	C83	6281 (8)	3182 (7)	6133 (6)	19 (3)*
O3	3508 (6)	2967 (5)	4533 (4)	20 (2)*	C84	5192 (8)	3628 (7)	5992 (6)	15 (3)*
C1	−2296 (8)	483 (6)	1318 (7)	21 (3)*	C85	4147 (9)	3787 (7)	6631 (6)	18 (3)*
C2	−2785 (8)	418 (7)	2208 (6)	20 (3)*	C86	3060 (8)	4177 (6)	6517 (5)	15 (3)*
C3	−1985 (8)	−44 (7)	2590 (6)	20 (3)*	C87	2024 (8)	4288 (7)	7147 (6)	22 (3)*
C4	−977 (8)	−279 (6)	1937 (6)	15 (3)*	C88	1179 (7)	4706 (6)	6793 (5)	13 (2)*
C5	84 (9)	−740 (7)	2074 (6)	22 (3)*	C89	1693 (8)	4846 (7)	5905 (5)	17 (3)*
C6	1063 (8)	−935 (6)	1394 (6)	16 (3)*	C90	1159 (8)	5287 (7)	5281 (6)	18 (3)*
C7	2136 (9)	−1478 (7)	1516 (6)	19 (3)*	C91	−335 (4)	6368 (4)	6164 (4)	21 (2)
C8	2900 (9)	−1494 (8)	768 (6)	24 (3)*	C92	−1504 (4)	6707 (4)	6490 (4)	28 (2)
C9	2371 (8)	−928 (7)	153 (6)	19 (2)*	C93	−2477 (4)	6321 (4)	6265 (4)	28 (2)
C10	2980 (7)	−768 (6)	−725 (5)	12 (3)*	C94	−2281 (4)	5595 (4)	5714 (4)	28 (2)
C11	2366 (8)	−313 (6)	−1288 (6)	16 (3)*	C95	−1112 (4)	5256 (4)	5389 (4)	19 (2)
C12	2958 (9)	−68 (7)	−2182 (6)	23 (3)*	C96	−139 (4)	5643 (4)	5614 (4)	16 (2)
C13	2154 (8)	367 (7)	−2562 (6)	21 (3)*	C97	4892 (5)	6236 (4)	1120 (3)	21 (2)
C14	1013 (8)	449 (7)	−1883 (6)	17 (3)*	C98	4932 (5)	6499 (4)	272 (3)	21 (2)
C15	−40 (7)	873 (6)	−2036 (5)	14 (3)*	C99	4096 (5)	6067 (4)	−59 (3)	25 (2)
C16	−1059 (9)	954 (7)	−1396 (6)	21 (3)*	C100	3218 (5)	5372 (4)	456 (3)	24 (2)
C17	−2176 (8)	1388 (7)	−1527 (6)	21 (3)*	C101	3178 (5)	5110 (4)	1303 (3)	22 (2)
C18	−2960 (8)	1405 (7)	−736 (6)	18 (3)*	C102	4014 (5)	5542 (4)	1635 (3)	19 (2)
C19	−2329 (8)	967 (7)	−144 (5)	17 (3)*	C103	9243 (5)	3797 (3)	3370 (4)	22 (2)
C20	−2848 (7)	898 (6)	728 (5)	12 (2)*	C104	10387 (5)	3379 (3)	3123 (4)	35 (2)
C21	−5111 (5)	630 (3)	1192 (4)	29 (2)	C105	10490 (5)	2341 (3)	3098 (4)	28 (2)
C22	−6277 (5)	1005 (3)	1446 (4)	33 (2)	C106	9449 (5)	1721 (3)	3321 (4)	36 (3)
C23	−6434 (5)	2023 (3)	1549 (4)	28 (2)	C107	8306 (5)	2139 (3)	3568 (4)	35 (3)
C24	−5424 (5)	2665 (3)	1397 (4)	30 (2)	C108	8203 (5)	3177 (3)	3593 (4)	15 (2)
C25	−4258 (5)	2290 (3)	1143 (4)	29 (2)	C109	4110 (8)	2361 (4)	7793 (4)	42 (3)
C26	−4102 (5)	1272 (3)	1041 (4)	21 (2)	C110	4134 (8)	2000 (4)	8614 (4)	53 (3)
C27	1068 (5)	−622 (4)	3208 (3)	19 (2)	C111	4227 (8)	2677 (4)	9166 (4)	36 (3)
C28	1137 (5)	−873 (4)	4034 (3)	31 (2)	C112	4296 (8)	3715 (4)	8896 (4)	57 (4)
C29	286 (5)	−1550 (4)	4601 (3)	25 (2)	C113	4272 (8)	4075 (4)	8074 (4)	52 (3)
C30	−632 (5)	−1974 (4)	4342 (3)	24 (2)	C114	4180 (8)	3398 (4)	7523 (4)	19 (2)
C31	−700 (5)	−1722 (4)	3515 (3)	21 (2)	C120	3888 (10)	6859 (8)	4644 (7)	34 (4)*
C32	150 (5)	−1046 (4)	2948 (3)	15 (2)	C121	4688 (13)	7799 (11)	4369 (14)	75 (8)*
C33	4503 (4)	−1806 (4)	−1591 (4)	17 (2)	C122	5949 (15)	7436 (12)	4192 (15)	90 (8)*
C34	5698 (4)	−2113 (4)	−1866 (4)	27 (2)	C123	5842 (11)	6425 (10)	4023 (13)	77 (7)*
C35	6599 (4)	−1715 (4)	−1573 (4)	27 (2)	C124	3365 (12)	2136 (8)	5191 (7)	35 (4)*
C36	6305 (4)	−1010 (4)	−1005 (4)	25 (2)	C125	3472 (13)	1201 (9)	4781 (8)	44 (5)*
C37	5110 (4)	−703 (4)	−730 (4)	26 (2)	C126	3128 (16)	1511 (10)	3970 (8)	54 (6)*
C38	4208 (4)	−1101 (4)	−1023 (4)	16 (2)	C127	3498 (11)	3588 (8)	3747 (7)	34 (4)*
C39	40 (6)	552 (3)	−3504 (4)	25 (2)	C130	7249 (19)	−514 (16)	6072 (14)	86 (6)
C40	44 (6)	916 (3)	−4330 (4)	24 (2)	C131	6578 (19)	294 (15)	6549 (13)	86 (5)
C41	−45 (6)	1950 (3)	−4567 (4)	26 (2)	C132	5547 (18)	478 (15)	6119 (13)	78 (5)
C42	−139 (6)	2620 (3)	−3978 (4)	29 (2)	C133	6327 (23)	460 (19)	5125 (16)	108 (7)
C43	−143 (6)	2257 (3)	−3152 (4)	26 (2)	C134	5574 (77)	−604 (59)	5830 (49)	353 (38)
C44	−53 (6)	1223 (3)	−2915 (4)	15 (2)	C140	8189 (15)	5397 (12)	9656 (11)	66 (4)
C50	626 (14)	1911 (10)	856 (8)	45 (5)*	C141	8380 (23)	5438 (18)	8741 (16)	109 (7)
C51	978 (13)	2984 (10)	667 (8)	49 (5)*	C142	8019 (28)	4450 (22)	8540 (19)	133 (10)
C52	732 (13)	3340 (8)	−164 (8)	42 (5)*	C143	7013 (27)	4273 (22)	9327 (19)	128 (9)
C53	751 (12)	2392 (8)	−564 (7)	39 (4)*	C144	7597 (14)	4418 (12)	9988 (10)	58 (4)

[a] Estimated standard deviations in the least significant digits are given in parentheses. [b] For values with asterisks, the equivalent isotropic U is defined as $^1/_3$ of the trace of the U_{ij} tensor.

Table III. Atomic Coordinates ($\times 10^4$) and Isotropic Thermal Parameters ($Å^2 \times 10^3$)[a] for **2**

atom	*x*	*y*	*z*	U_{iso}[b]	atom	*x*	*y*	*z*	U_{iso}[b]
Fe	0	0	0	12 (1)*	C60	1635 (9)	−2364 (7)	−2664 (5)	23 (3)*
Ga	4080 (1)	4490 (1)	4571 (1)	18 (1)*	C61	2023 (9)	−1831 (7)	−3518 (7)	29 (3)*
Cu	539 (1)	−2670 (1)	−764 (1)	29 (1)*	C62	2366 (8)	−3100 (6)	−2406 (5)	20 (3)*
N1	−1150 (7)	47 (5)	1165 (5)	22 (2)*	C63	3499 (10)	−3378 (7)	−2998 (7)	35 (4)*
N2	1234 (6)	−618 (5)	549 (4)	17 (2)*	C64	−745 (9)	−3009 (8)	1184 (8)	39 (4)*
N3	1196 (6)	50 (5)	−1125 (4)	15 (2)*	C65	−1155 (11)	−3452 (8)	1996 (8)	42 (4)*
N4	−1184 (7)	714 (6)	−542 (5)	19 (2)*	C66	−2573 (9)	−1990 (8)	1380 (7)	37 (4)*
N5	5317 (7)	3878 (6)	5150 (5)	19 (2)*	C67	−1415 (10)	−2255 (8)	885 (7)	34 (3)*
N6	5266 (7)	4444 (5)	3442 (4)	19 (2)*	C71	5184 (8)	3632 (7)	6009 (6)	22 (3)*
N7	2810 (6)	5046 (5)	4025 (4)	18 (1)*	C72	6274 (8)	3190 (8)	6141 (7)	26 (3)*
N8	2886 (7)	4512 (6)	5727 (5)	23 (3)*	C73	7057 (9)	3124 (8)	5386 (7)	31 (3)*
N9	2256 (8)	−1410 (7)	−4180 (6)	37 (3)*	C74	6451 (8)	3558 (6)	4765 (5)	19 (3)*
N10	4405 (9)	−3552 (8)	−3379 (7)	49 (4)*	C75	6978 (8)	3590 (7)	3886 (6)	19 (3)*
N11	−1445 (11)	−3810 (7)	2728 (6)	53 (4)*	C76	6390 (7)	4023 (6)	3290 (5)	17 (2)*
N12	−3537 (11)	−1800 (9)	1786 (10)	70 (5)*	C77	6921 (8)	4098 (7)	2387 (5)	22 (3)*
S1	−900 (2)	−1578 (2)	−146 (2)	36 (1)*	C78	6126 (8)	4578 (6)	2017 (5)	23 (3)*
S2	313 (2)	−1983 (2)	−2005 (2)	31 (1)*	C79	5083 (8)	4770 (6)	2675 (5)	20 (3)*
S3	2008 (2)	−3674 (2)	−1372 (2)	27 (1)*	C80	4024 (8)	5214 (6)	2544 (6)	21 (3)*
S4	560 (3)	−3421 (2)	551 (2)	44 (1)*	C81	2986 (8)	5347 (7)	3168 (6)	23 (3)*
O1	627 (6)	1530 (5)	95 (4)	26 (2)*	C82	1944 (8)	5863 (7)	3026 (5)	21 (3)*
O2	3486 (6)	2978 (5)	4549 (4)	26 (2)*	C83	1111 (8)	5869 (7)	3807 (5)	20 (3)*
O3	4702 (6)	5973 (5)	4558 (5)	37 (3)*	C84	1668 (8)	5360 (7)	4431 (5)	22 (3)*
C1	−2283 (8)	484 (7)	1330 (6)	21 (3)*	C85	1146 (8)	5259 (7)	5306 (6)	22 (3)*
C2	−2784 (8)	410 (7)	2209 (6)	23 (3)*	C86	1701 (7)	4837 (6)	5905 (5)	17 (2)*
C3	−1980 (8)	−41 (7)	2602 (6)	22 (3)*	C87	1168 (8)	4716 (7)	6793 (6)	21 (3)*
C4	−953 (8)	−279 (6)	1939 (5)	21 (3)*	C88	2029 (8)	4311 (7)	7163 (6)	23 (3)*
C5	79 (8)	−748 (6)	2074 (5)	19 (3)*	C89	3077 (8)	4179 (7)	6519 (5)	19 (3)*
C6	1080 (8)	−919 (6)	1401 (5)	16 (3)*	C90	4125 (8)	3770 (6)	6658 (5)	19 (3)*
C7	2127 (8)	−1490 (6)	1535 (5)	22 (3)*	C91	4100 (8)	2369 (5)	7809 (4)	47 (3)
C8	2905 (8)	−1496 (8)	768 (5)	25 (3)*	C92	4135 (8)	2012 (4)	8629 (4)	57 (3)
C9	2377 (8)	−938 (6)	164 (6)	20 (2)*	C93	4245 (8)	2692 (4)	9169 (4)	51 (3)
C10	2940 (8)	−781 (7)	−708 (5)	20 (3)*	C94	4320 (8)	3727 (4)	8890 (4)	62 (4)
C11	2371 (8)	−322 (6)	−1295 (6)	21 (3)*	C95	4285 (8)	4084 (4)	8070 (4)	51 (3)
C12	2948 (8)	−89 (7)	−2189 (5)	20 (3)*	C96	4175 (8)	3404 (4)	7529 (4)	26 (2)
C13	2133 (9)	377 (7)	−2553 (5)	24 (3)*	C97	8298 (5)	2130 (4)	3564 (5)	37 (2)
C14	1015 (8)	437 (7)	−1878 (6)	23 (3)*	C98	9441 (5)	1713 (4)	3311 (5)	40 (2)
C15	−33 (7)	875 (6)	−2026 (5)	19 (3)*	C99	10481 (5)	2331 (4)	3096 (5)	30 (2)
C16	−1077 (8)	969 (6)	−1390 (5)	19 (3)*	C100	10378 (5)	3366 (4)	3133 (5)	37 (2)
C17	−2150 (8)	1408 (7)	−1518 (5)	20 (3)*	C101	9235 (5)	3782 (4)	3385 (5)	31 (2)
C18	−2966 (7)	1416 (6)	−739 (5)	14 (2)*	C102	8195 (5)	3164 (4)	3600 (5)	20 (2)
C19	−2315 (8)	996 (7)	−126 (6)	20 (3)*	C103	4875 (5)	6246 (4)	1134 (3)	24 (2)
C20	−2863 (7)	883 (6)	748 (6)	20 (3)*	C104	4934 (5)	6501 (4)	283 (3)	29 (2)
C21	−5114 (5)	624 (3)	1201 (5)	32 (2)	C105	4118 (5)	6058 (4)	−55 (3)	32 (2)
C22	−6279 (5)	1002 (3)	1443 (5)	36 (2)	C106	3242 (5)	5359 (4)	458 (3)	27 (2)
C23	−6436 (5)	2018 (3)	1540 (5)	30 (2)	C107	3183 (5)	5103 (4)	1309 (3)	25 (2)
C24	−5427 (5)	2657 (3)	1395 (5)	36 (2)	C108	3999 (5)	5546 (4)	1647 (3)	23 (2)
C25	−4261 (5)	2279 (3)	1153 (5)	32 (2)	C109	−333 (4)	6358 (4)	6177 (4)	26 (2)
C26	−4105 (5)	1262 (3)	1056 (5)	23 (2)	C110	−1505 (4)	6690 (4)	6501 (4)	30 (2)
C27	−695 (5)	−1731 (4)	3522 (4)	26 (2)	C111	−2471 (4)	6301 (4)	6274 (4)	31 (2)
C28	−624 (5)	−1995 (4)	4346 (4)	28 (2)	C112	−2265 (4)	5579 (4)	5724 (4)	32 (2)
C29	290 (5)	−1573 (4)	4607 (4)	30 (2)	C113	−1093 (4)	5246 (4)	5401 (4)	26 (2)
C30	1134 (5)	−887 (4)	4043 (4)	35 (2)	C114	−127 (4)	5636 (4)	5627 (4)	20 (2)
C31	1063 (5)	−624 (4)	3219 (4)	25 (2)	C120	3349 (13)	2132 (8)	5210 (7)	38 (4)*
C32	148 (5)	−1045 (4)	2958 (4)	23 (2)	C121	3453 (12)	1194 (9)	4796 (8)	46 (5)*
C33	4498 (4)	−1803 (4)	−1580 (4)	24 (2)	C122	3102 (14)	1526 (8)	3987 (8)	52 (5)*
C34	5690 (4)	−2111 (4)	−1862 (4)	29 (2)	C123	3441 (11)	2615 (8)	3786 (7)	35 (4)*
C35	6598 (4)	−1719 (4)	−1576 (4)	29 (2)	C130	3922 (9)	6844 (7)	4663 (7)	34 (3)*
C36	6313 (4)	−1018 (4)	−1008 (4)	30 (2)	C131	4700 (14)	7755 (11)	4397 (12)	68 (6)*
C37	5120 (4)	−709 (4)	−726 (4)	30 (2)	C132	5992 (17)	7386 (12)	4226 (15)	94 (9)*
C38	4213 (4)	−1102 (4)	−1012 (4)	19 (2)	C133	5848 (11)	6351 (9)	4104 (11)	60 (6)*
C39	29 (6)	550 (3)	−3499 (4)	31 (2)	C140	7938 (32)	4460 (26)	−1455 (23)	152 (11)
C40	17 (6)	910 (3)	−4323 (4)	32 (2)	C141	7091 (31)	4158 (26)	−614 (22)	148 (11)
C41	−68 (6)	1943 (3)	−4566 (4)	29 (2)	C142	7586 (14)	4406 (12)	13 (10)	60 (4)
C42	−142 (6)	2615 (3)	−3985 (4)	35 (2)	C143	8236 (17)	5361 (14)	−335 (12)	79 (5)
C43	−130 (6)	2255 (3)	−3161 (4)	32 (2)	C144	8317 (25)	5466 (21)	−1239 (18)	118 (8)
C44	−44 (6)	1222 (3)	−2918 (4)	18 (2)	C150	6594 (21)	271 (18)	6535 (15)	98 (6)
C50	599 (13)	1889 (9)	891 (7)	48 (5)*	C151	5571 (18)	483 (15)	6099 (13)	80 (5)
C51	955 (16)	2965 (10)	672 (8)	62 (6)*	C152	6282 (23)	530 (20)	5143 (17)	112 (8)
C52	761 (15)	3305 (9)	−162 (8)	51 (5)*	C153	7250 (55)	−238 (45)	5211 (38)	248 (23)
C53	761 (11)	2378 (8)	−553 (7)	38 (4)*	C154	7210 (21)	−575 (18)	6089 (15)	98 (6)

[a] Estimated standard deviations in the least significant digits are given in parentheses. [b] For values with asterisks, the equivalent isotropic *U* is defined as $^1/_3$ of the trace of the U_{ij} tensor.

Table IV. Atomic Coordinates (×10⁴) and Isotropic Thermal Parameters (Å² × 10³)[a] for **3**

atom	x	y	z	U_{iso}[b]	atom	x	y	z	U_{iso}[b]
Fe	0	0	0	23 (1)*	C61	2435 (11)	−3093 (7)	−2501 (6)	38 (3)*
Al	4084 (2)	4450 (2)	4674 (1)	12 (1)*	C62	3529 (9)	−3395 (6)	−3122 (5)	26 (3)*
Cu	576 (1)	−2670 (1)	−862 (1)	40 (1)*	C63	2075 (8)	−1838 (6)	−3664 (6)	28 (3)*
N1	−1169 (6)	721 (5)	−553 (4)	24 (2)*	C64	−748 (11)	−2972 (8)	1002 (7)	43 (4)*
N2	−1128 (6)	59 (5)	1142 (5)	25 (2)*	C65	−1171 (15)	−3433 (9)	1836 (9)	62 (5)*
N3	1241 (7)	−606 (5)	568 (4)	23 (2)*	C66	−1331 (10)	−2217 (7)	750 (7)	39 (3)*
N4	1225 (6)	51 (5)	−1112 (5)	23 (2)*	C67	−2516 (12)	−1910 (8)	1222 (8)	52 (4)*
N5	2848 (7)	5036 (5)	4105 (4)	25 (2)*	C71	6359 (7)	3994 (7)	3395 (6)	26 (3)*
N6	5246 (7)	4401 (5)	3549 (4)	24 (2)*	C72	6885 (8)	4055 (7)	2496 (6)	26 (3)*
N7	5260 (7)	3785 (5)	5244 (4)	25 (2)*	C73	6124 (9)	4531 (7)	2114 (6)	31 (3)*
N8	2889 (7)	4452 (5)	5793 (4)	24 (2)*	C74	5055 (7)	4756 (6)	2761 (5)	21 (2)*
N9	2305 (12)	−1408 (9)	−4255 (7)	67 (5)	C75	4064 (8)	5202 (6)	2607 (5)	24 (3)*
N10	4286 (11)	−3593 (8)	−3599 (6)	56 (4)*	C76	3022 (7)	5332 (6)	3272 (5)	23 (3)*
N11	−3467 (10)	−1691 (9)	1549 (8)	68 (4)*	C77	1974 (9)	5851 (7)	3122 (6)	30 (3)*
N12	−1512 (16)	−3821 (10)	2559 (9)	86 (6)*	C78	1185 (9)	5855 (7)	3877 (6)	30 (3)*
S1	−820 (2)	−1571 (2)	−245 (2)	39 (1)*	C79	1723 (8)	5353 (6)	4490 (6)	27 (3)*
S2	548 (4)	−3452 (3)	422 (2)	77 (1)*	C80	1185 (8)	5224 (7)	5353 (6)	28 (3)*
S3	2102 (3)	−3636 (2)	−1492 (2)	45 (1)*	C81	1724 (8)	4806 (7)	5963 (5)	25 (3)*
S4	408 (3)	−1957 (2)	−2114 (2)	43 (1)*	C82	1199 (8)	4661 (7)	6830 (6)	31 (3)*
O1	625 (7)	1539 (5)	129 (4)	38 (2)*	C83	2006 (9)	4213 (7)	7231 (6)	31 (3)*
O2	4689 (7)	5722 (5)	4800 (4)	40 (2)*	C84	3066 (9)	4105 (6)	6582 (5)	28 (3)*
O3	3499 (6)	3039 (4)	4566 (4)	28 (2)*	C85	4128 (9)	3697 (7)	6722 (5)	28 (3)*
C1	−1043 (8)	948 (6)	−1415 (5)	25 (3)*	C86	5155 (8)	3566 (7)	6088 (6)	26 (3)*
C2	−2125 (8)	1394 (7)	−1541 (5)	28 (3)*	C87	6249 (9)	3135 (8)	6233 (7)	35 (3)*
C3	−2915 (5)	1391 (7)	−778 (6)	26 (3)*	C88	7015 (9)	3063 (7)	5467 (6)	32 (3)*
C4	−2299 (8)	999 (7)	−158 (5)	26 (3)*	C89	6429 (7)	3477 (6)	4841 (6)	23 (3)*
C5	−2814 (7)	924 (6)	699 (5)	23 (3)*	C90	6924 (8)	3567 (7)	3987 (6)	29 (3)*
C6	−2238 (8)	496 (6)	1307 (5)	25 (3)*	C91	8307 (5)	2127 (4)	3693 (5)	41 (2)
C7	−2749 (10)	460 (8)	2207 (7)	42 (4)*	C92	9454 (5)	1739 (4)	3409 (5)	44 (3)
C8	−1931 (7)	1 (7)	2580 (6)	28 (3)*	C93	10447 (5)	2379 (4)	3131 (5)	39 (2)
C9	−966 (8)	−250 (6)	1910 (5)	25 (3)*	C94	10293 (5)	3407 (4)	3135 (5)	47 (3)
C10	103 (8)	−751 (7)	2051 (5)	25 (3)*	C95	9147 (5)	3794 (4)	3419 (5)	34 (2)
C11	1080 (9)	−950 (6)	1421 (6)	31 (3)*	C96	8154 (5)	3154 (4)	3698 (5)	29 (2)
C12	2117 (9)	−1482 (7)	1533 (6)	32 (3)*	C97	4889 (5)	6234 (5)	1251 (4)	31 (2)
C13	2899 (10)	−1475 (8)	786 (6)	37 (3)*	C98	4924 (5)	6516 (5)	408 (4)	44 (3)
C14	2380 (8)	−927 (7)	164 (5)	25 (3)*	C99	4102 (5)	6106 (5)	40 (4)	50 (3)
C15	2948 (8)	−781 (7)	−696 (5)	25 (3)*	C100	3246 (5)	5414 (5)	516 (4)	41 (2)
C16	2347 (8)	−308 (6)	−1281 (5)	27 (3)*	C101	3211 (5)	5131 (5)	1359 (4)	33 (2)
C17	2955 (8)	−96 (7)	−2175 (5)	28 (3)*	C102	4033 (5)	5541 (5)	1727 (4)	34 (2)
C18	2160 (8)	338 (7)	−2520 (6)	32 (3)*	C103	−329 (5)	6338 (5)	6220 (4)	34 (2)
C19	1046 (8)	449 (6)	−1892 (5)	23 (3)*	C104	−1496 (5)	6689 (5)	6493 (4)	37 (2)
C20	10 (8)	859 (6)	−2033 (6)	26 (3)*	C105	−2422 (5)	6309 (5)	6207 (4)	42 (2)
C21	−114 (7)	2275 (4)	−3096 (3)	34 (2)	C106	−2182 (5)	5577 (5)	5648 (4)	45 (3)
C22	−134 (7)	2657 (4)	−3911 (3)	43 (2)	C107	−1015 (5)	5226 (5)	5375 (4)	30 (2)
C23	−44 (7)	2016 (4)	−4537 (3)	34 (2)	C108	−89 (5)	5606 (5)	5661 (4)	24 (2)
C24	65 (7)	992 (4)	−4347 (3)	40 (2)	C109	4263 (8)	4002 (4)	8188 (5)	52 (3)
C25	84 (7)	610 (4)	−3532 (3)	33 (2)	C110	4303 (8)	3642 (4)	9004 (5)	68 (4)
C26	−5 (7)	1252 (4)	−2906 (3)	25 (2)	C111	4218 (8)	2620 (4)	9250 (5)	53 (3)
C27	−5037 (6)	667 (4)	1245 (5)	40 (2)	C112	4092 (8)	1957 (4)	8679 (5)	61 (3)
C28	−6192 (6)	1035 (4)	1535 (5)	48 (3)	C113	4052 (8)	2317 (4)	7863 (5)	56 (3)
C29	−6360 (6)	2053 (4)	1603 (5)	49 (3)	C114	4137 (8)	3340 (4)	7617 (5)	32 (2)
C30	−5373 (6)	2702 (4)	1380 (5)	49 (3)	C130	3296 (11)	2197 (7)	5238 (7)	39 (4)*
C31	−4218 (6)	2334 (4)	1089 (5)	41 (2)	C131	3439 (14)	1272 (8)	4780 (7)	54 (5)*
C32	−4050 (6)	1316 (4)	1021 (5)	29 (2)	C132	3075 (14)	1636 (8)	3962 (7)	55 (5)*
C33	976 (5)	−638 (4)	3265 (3)	33 (2)	C133	3428 (13)	2664 (8)	3802 (7)	50 (4)*
C34	996 (5)	−901 (4)	4102 (3)	37 (2)	C140	7243 (17)	−547 (14)	6133 (12)	82 (5)
C35	161 (5)	−1589 (4)	4610 (3)	43 (3)	C141	6517 (21)	219 (17)	6583 (14)	102 (6)
C36	−695 (5)	−2013 (4)	4281 (3)	40 (2)	C142	5564 (20)	450 (16)	6038 (14)	100 (6)
C37	−716 (5)	−1750 (4)	3444 (3)	38 (2)	C143	6279 (15)	431 (12)	5171 (10)	70 (4)
C38	120 (5)	−1062 (4)	2936 (3)	27 (2)	C144	7337 (30)	−134 (25)	5310 (20)	149 (10)
C39	5117 (5)	−695 (4)	−682 (4)	32 (2)	C150	4982 (10)	7224 (8)	3655 (7)	37 (2)
C40	6297 (5)	−1020 (4)	−951 (4)	37 (2)	C151	4034 (16)	7746 (13)	3436 (11)	78 (4)
C41	6571 (5)	−1746 (4)	−1515 (4)	41 (2)	C152	4332 (17)	8835 (14)	3452 (11)	82 (5)
C42	5664 (5)	−2146 (4)	−1810 (4)	40 (2)	C153	5134 (20)	8791 (16)	4007 (14)	97 (6)
C43	4485 (5)	−1822 (4)	−1540 (4)	31 (2)	C154	5902 (20)	7844 (16)	3808 (14)	98 (6)
C44	4211 (5)	−1096 (4)	−976 (4)	28 (2)	C160	8092 (34)	5486 (27)	8791 (24)	172 (13)
C50	733 (13)	2374 (8)	−504 (7)	50 (4)*	C161	8559 (33)	4188 (25)	8402 (22)	155 (11)
C51	836 (15)	3269 (10)	−108 (9)	63 (5)*	C162	7442 (45)	4077 (36)	9175 (31)	230 (18)
C52	949 (22)	2938 (10)	776 (9)	88 (8)*	C163	7653 (27)	4321 (23)	9956 (19)	134 (9)
C53	754 (21)	1894 (10)	897 (9)	88 (8)*	C164	8171 (48)	5277 (37)	9697 (35)	241 (20)
C60	1725 (9)	−2349 (7)	−2778 (6)	31 (3)*					

[a] Estimated standard deviations in the least significant digits are given in parentheses. [b] For values with asterisks, the equivalent isotropic U is defined as $^1/_3$ of the trace of the U_{ij} tensor.

the crystal showed signs of cracking at −70 °C. To avoid this problem, the diffraction data for **3** were collected at −60 °C.

Results from the room-temperature X-ray structure determination for **1** were reported in a previous communication.[11] Herein, the low-temperature X-ray structure determination of **1** is reported. The structure of **1** had been solved from the room-temperature data by using the direct

Table V. Selected Bond Lengths (Å)[a] and Angles (deg)[a] for **1** at −130 °C

Cu–S1	2.307 (3)	C4–C5	1.416 (14)	N5–C74	1.394 (12)	N12–C67	1.062 (13)	Fe1–O1	2.212 (7)	C81–C82	1.467 (14)
Cu–S2	2.268 (3)	C5–C6	1.408 (12)	N6–C86	1.403 (12)	S1–Fe1	2.411 (3)	O1–C50	1.432 (16)	C82–C83	1.328 (13)
Cu–S3	2.246 (3)	C6–C7	1.468 (13)	N6–C89	1.386 (11)	Fe1–N1	2.005 (7)	O1–C53	1.451 (12)	C83–C84	1.439 (14)
Cu–S4	2.236 (3)	C7–C8	1.313 (12)	N7–C81	1.389 (11)	Fe1–N2	2.007 (9)	C50–C51	1.463 (18)	C84–C85	1.402 (12)
S1–C60	1.764 (10)	C8–C9	1.451 (14)	N7–C84	1.370 (12)	Fe1–N3	1.984 (7)	C51–C52	1.501 (20)	C85–C86	1.395 (14)
S2–C62	1.723 (10)	C9–C10	1.425 (11)	N8–C76	1.358 (12)	Fe1–N4	1.993 (7)	C52–C53	1.503 (17)	C86–C87	1.372 (12)
S3–C64	1.740 (11)	C10–C11	1.393 (13)	N8–C79	1.364 (11)	N1–C1	1.405 (11)	O2–C120	1.448 (13)	C87–C88	1.346 (14)
S4–C66	1.723 (10)	C11–C12	1.450 (12)	C71–C72	1.424 (13)	N1–C4	1.396 (12)	O2–C123	1.419 (14)	C88–C89	1.420 (12)
C60–C61	1.461 (14)	C12–C13	1.341 (15)	C72–C73	1.402 (14)	N2–C6	1.362 (12)	C120–C121	1.507 (18)	C89–C90	1.405 (14)
C60–C62	1.327 (16)	C13–C14	1.490 (11)	C73–C74	1.424 (13)	N2–C9	1.380 (11)	C121–C122	1.482 (23)	C71–C90	1.409 (12)
C62–C63	1.421 (16)	C14–C15	1.398 (13)	C74–C75	1.378 (11)	N3–C11	1.394 (11)	C122–C123	1.429 (23)	Fe2–O3	2.175 (7)
N9–C61	1.150 (15)	C15–C16	1.361 (12)	C75–C76	1.399 (13)	N3–C14	1.370 (13)	O2–Fe2	2.140 (7)	O3–C124	1.427 (12)
N10–C63	1.172 (16)	C16–C17	1.458 (15)	C76–C77	1.459 (12)	N4–C16	1.385 (12)	Fe2–N5	2.046 (9)	O3–C127	1.468 (14)
C64–C65	1.459 (13)	C17–C18	1.378 (12)	C77–C78	1.351 (14)	N4–C19	1.358 (11)	Fe2–N6	2.041 (6)	C124–C125	1.488 (17)
C64–C66	1.365 (15)	C18–C19	1.436 (14)	C78–C79	1.444 (12)	C1–C2	1.422 (14)	Fe2–N7	2.037 (9)	C125–C126	1.513 (21)
C66–C67	1.452 (14)	C19–C20	1.400 (11)	C79–C80	1.418 (14)	C2–C3	1.351 (14)	Fe2–N8	2.036 (7)	C126–C127	1.473 (17)
N11–C65	1.037 (14)	C1–C20	1.364 (14)	C80–C81	1.383 (13)	C3–C4	1.417 (12)	N5–C71	1.350 (11)		

S1–Cu–S2	89.7 (1)	S1–Cu–S3	176.3 (1)	O1–Fe1–N2	90.4 (3)	O1–Fe1–N3	90.0 (3)
S1–Cu–S4	87.7 (1)	S2–Cu–S3	91.1 (1)	O1–Fe1–N4	85.4 (3)	Fe1–O1–C50	125.6 (6)
S2–Cu–S4	173.8 (1)	S3–Cu–S4	91.9 (1)	Fe1–O1–C53	124.7 (7)	O1–C50–C51	109.2 (10)
Cu–S1–C60	98.5 (4)	Cu–S2–C62	101.6 (4)	O1–C53–C52	108.0 (9)	C50–O1–C53	107.9 (8)
Cu–S3–C64	100.4 (3)	Cu–S4–C66	99.6 (4)	C50–C51–C52	105.5 (12)	C51–C52–C53	104.2 (10)
S1–C60–C61	115.6 (8)	S1–C60–C62	123.6 (8)	O2–C120–C121	105.8 (9)	O2–C123–C122	107.7 (13)
S2–C62–C60	122.3 (8)	S2–C62–C63	115.6 (8)	C120–O2–C123	106.5 (8)	C120–C121–C122	105.4 (12)
C60–C62–C63	122.1 (10)	C60–C61–N9	179.0 (16)	C121–C122–C123	103.8 (14)	C120–O2–Fe2	122.8 (6)
C61–C60–C62	120.8 (9)	C62–C63–N10	176.0 (13)	C123–O2–Fe2	124.0 (8)	O2–Fe2–N5	89.0 (3)
S3–C64–C66	120.8 (7)	S3–C64–C65	117.3 (8)	O2–Fe2–N6	92.1 (3)	O2–Fe2–N7	93.9 (3)
S4–C66–C64	124.0 (8)	S4–C66–C67	116.4 (8)	O2–Fe2–N8	88.4 (3)	N5–Fe2–N6	89.4 (3)
C64–C65–N11	179.2 (5)	C64–C66–C67	119.6 (9)	N5–Fe2–N7	177.0 (3)	N5–Fe2–N8	90.9 (3)
C65–C64–C66	121.5 (9)	C66–C67–N12	174.7 (12)	N6–Fe2–N7	89.5 (3)	N6–Fe2–N8	179.4 (3)
Cu–S1–Fe1	112.5 (1)	C65–S1–Fe1	106.7 (4)	N7–Fe2–N8	90.1 (3)	Fe2–N5–C71	127.3 (7)
S1–Fe1–O1	172.3 (2)	S1–Fe1–N1	92.9 (2)	Fe2–N5–C74	125.0 (6)	Fe2–N6–C86	127.3 (5)
S1–Fe1–N2	97.2 (2)	S1–Fe1–N3	91.5 (2)	Fe2–N6–C89	127.7 (6)	Fe2–N7–C81	125.9 (6)
S1–Fe1–N4	87.1 (2)	N1–Fe1–N2	88.9 (3)	Fe2–N7–C84	127.6 (6)	Fe2–N8–C76	125.3 (6)
N1–Fe1–N3	175.6 (3)	N1–Fe1–N4	90.6 (3)	Fe2–N8–C79	126.5 (6)	C71–N5–C74	106.7 (8)
N2–Fe1–N3	90.6 (3)	N2–Fe1–N4	175.7 (3)	N5–C71–C72	111.0 (7)	N5–C71–C90	124.9 (9)
N3–Fe1–N4	89.7 (3)	Fe1–N1–C1	126.2 (6)	C71–C72–C73	106.2 (7)	C72–C73–C74	106.4 (8)
Fe1–N1–C4	129.1 (6)	Fe1–N2–C6	126.9 (6)	N5–C74–C73	109.6 (7)	N5–C74–C75	125.9 (9)
Fe1–N2–C9	126.2 (6)	Fe1–N3–C11	126.2 (6)	C73–C74–C75	124.1 (8)	C74–C75–C76	125.2 (8)
Fe1–N3–C14	126.5 (6)	Fe1–N4–C16	127.1 (6)	C76–N8–C79	107.9 (7)	N8–C76–C75	127.0 (7)
Fe1–N4–C19	126.5 (6)	C1–N1–C4	104.7 (7)	N8–C76–C77	108.6 (8)	C75–C76–C77	124.4 (8)
N1–C1–C2	108.7 (9)	N1–C1–C20	125.4 (8)	C76–C77–C78	107.1 (8)	C77–C78–C79	106.9 (8)
C1–C2–C3	109.2 (8)	C2–C3–C4	106.4 (8)	N8–C79–C78	109.4 (8)	N8–C79–C80	126.5 (8)
N1–C4–C3	111.0 (8)	N1–C4–C5	124.8 (7)	C78–C79–C80	124.1 (8)	C79–C80–C81	123.8 (8)
C3–C4–C5	124.2 (9)	C4–C5–C6	121.2 (9)	C81–N7–C84	106.4 (8)	N7–C81–C80	126.9 (9)
C6–N2–C9	106.2 (8)	N2–C6–C5	128.2 (9)	N7–C81–C82	108.2 (7)	C80–C81–C82	124.9 (8)
N2–C6–C7	109.2 (7)	C5–C6–C7	122.4 (9)	C81–C82–C83	107.6 (8)	C82–C83–C84	107.7 (9)
C6–C7–C8	107.5 (9)	C7–C8–C9	107.5 (9)	N7–C84–C83	110.1 (7)	N7–C84–C85	125.2 (9)
N2–C9–C8	109.5 (7)	N2–C9–C10	128.0 (9)	C83–C84–C85	124.8 (9)	C84–C85–C86	126.3 (9)
C8–C9–C10	122.5 (8)	C9–C10–C11	119.3 (7)	C86–N6–C89	105.0 (7)	N6–C86–C85	124.0 (7)
C11–N3–C14	107.3 (7)	N3–C11–C10	129.3 (8)	N6–C86–C87	110.2 (8)	C85–C86–C87	125.8 (9)
N3–C11–C12	108.6 (8)	C10–C11–C12	122.0 (8)	C86–C87–C88	108.4 (8)	C87–C88–C89	107.7 (7)
C11–C12–C13	108.7 (8)	C12–C13–C14	106.3 (8)	N6–C89–C88	108.8 (8)	N6–C89–C90	123.7 (7)
N3–C14–C13	108.9 (8)	N3–C14–C15	127.9 (7)	C88–C89–C90	127.8 (8)	C89–C90–C71	126.7 (8)
C13–C14–C15	123.2 (9)	C14–C15–C16	121.5 (9)	C90–C71–C72	123.9 (8)	N5–Fe2–O3	90.2 (3)
C16–N4–C19	106.2 (8)	N4–C16–C15	126.9 (9)	N6–Fe2–O3	91.1 (3)	N7–Fe2–O3	87.1 (3)
N4–C16–C17	109.7 (8)	C15–C16–C17	123.3 (9)	N8–Fe2–O3	88.4 (3)	O2–Fe2–O3	176.6 (3)
C16–C17–C18	106.2 (9)	C17–C18–C19	106.5 (8)	Fe2–O3–C124	126.3 (7)	Fe2–O3–C127	122.9 (5)
N4–C19–C18	111.4 (7)	N4–C19–C20	126.6 (9)	O3–C124–C125	106.5 (9)	O3–C127–C126	106.8 (9)
C18–C19–C20	121.8 (8)	C19–C20–C1	124.3 (8)	C124–O3–C127	109.4 (8)	C124–C125–C126	104.8 (10)
C20–C1–C2	125.9 (8)	O1–Fe1–N1	85.6 (3)	C125–C126–C127	103.7 (12)		

[a] Estimated standard deviations in the least significant digits are given in parentheses.

methods routine RANT.[16] For the low-temperature structure determination of **1**, the atom coordinates from the room temperature results were used as a starting point for refinement; starting points for the structures of **2** and **3** were provided by the heavy-atom coordinates determined from the Patterson syntheses.

Neutral-atom scattering factors and anomalous scattering contributions were employed for all atoms.[17] In the final structural models for **1** (at 20 and −130 °C), the phenyl groups of the porphyrin macrocycles were refined as rigid hexagons (C–C = 1.39 Å) to limit the number of adjustable parameters and keep the ratio of data points to parameters acceptably high. Anisotropic thermal parameters were used for all non-hydrogen atoms, except for those of the rigid phenyl groups and the occluded THF molecules. Hydrogen atoms of the porphyrin cores and the coordinated THF molecules were included in calculated positions (C–H = 0.96 Å, $U(H) = 1.2U_{iso}(C)$); no hydrogen atoms were included on the phenyl groups due to a software limitation on the total number of atoms. At convergence for the −130 °C structure (weighted least-squares refinement on F, $(\text{shift/esd})_{av} < 0.1$ over the last 10 cycles) the highest peak in the difference electron density map (2.6 e Å^{-3}) was located near the

(16) Calculations for diffractometer operations were performed by using software supplied with the Nicolet R3m diffractometer. All structural calculations were performed with the SHELXTL program library written by G. M. Sheldrick and supplied by Siemens Analytical X-Ray Corp., Madison, WI.

(17) *International Tables for X-Ray Crystallography*; Kynoch: Birmingham, England, 1974; Vol. IV, pp 99, 149.

coordinated THF molecule containing O2. This peak results from disorder in this ligand; this disorder was not modeled due to software limitations on the total number of atoms. The minimum in the electron density map was –0.62 e Å^{-3}.

The final structural models for **2** and **3** were constructed in a similar fashion as for **1**. At convergence for **2** (weighted least-squares refinement on F, $(\text{shift/esd})_{av} < 0.03$ over the last 10 cycles) the highest peak in the ΔF map (2.7 e Å^{-3}) was located within 0.02 Å of the Fe atom; the minimum in the map was –1.7 e Å^{-3}. At convergence for **3** (weighted least-squares refinement on F, $(\text{shift/esd})_{av} < 0.03$ over the last 10 cycles) the highest peak in the ΔF map (2.4 e Å^{-3}) was located near the coordinated H_2O molecule and appears to be due to a second H_2O molecule hydrogen bonded to the first with approximately 20% occupancy (based on refinement of the site occupancy factor). However, a satisfactory value of the isotropic thermal parameter for this atom was not obtained, and this partial atom was not included in the final refinement cycles. The minimum in the electron density map was –0.69 e Å^{-3}.

Significant disorder between the Al and Fe sites in **3** should have caused abnormal thermal parameters for these atoms, and this was not found to be the case. Two tests for possible disorder between the Ga and Fe sites in **2** were performed. In the first test, the identities assigned to the two metals were switched. Refinement resulted in a doubling of the equivalent isotropic thermal parameter for the "Ga" site and an unreasonable set of values for the thermal parameters of the "Fe" atom. In the second test, both metals were assigned as copper atoms and the site occupancy factors (SOF) of these two "Cu" atoms were refined. The SOF value for the atom at the Fe site decreased to 0.86, while that for the atom at the Ga site increased to 1.01. The ratio of these two values (1.17) is close to the ratio of the atomic numbers of gallium and iron (1.19), indicating that any disorder present between the Fe and Ga atoms is small. The excess electron density at the Fe site in the final ΔF map (see above) may indicate a small amount of such disorder.

The final fractional atomic coordinates for non-hydrogen atoms from the low-temperature structure determinations may be found in Tables II–IV. Selected bond lengths and angles involving the porphyrin cores, the metal atoms, the MNT^{2-} groups, and the metal-bound H_2O and THF molecules may be found in Tables V–VII. Tables of crystal data, anisotropic thermal parameters, and calculated hydrogen atom positions have been included as supplementary material.

Magnetic Susceptibility. Magnetic susceptibility and magnetization data for **2** and **3** were collected with the use of a Foner-type[18] Princeton Applied Research Model 155 vibrating-sample magnetometer (VSM). The VSM magnet (Magnion H-96), power supply (Magnion HSR-1365), and associated field control unit (Magnion FFC-4 with Rawson-Lush Model 920 MCM rotating-coil gaussmeter) were calibrated by using procedures described earlier.[19] The VSM was calibrated with Hg[Co(NCS)$_4$].[20,21] Temperatures were measured with a calibrated GaAs diode.[22] The data were corrected for diamagnetism of the constituent atoms by using Pascal's constants,[23,24] with a diamagnetic correction for TPP^{2-} of -700×10^{-6} cgs units.[25] The samples (~100 mg each) were ground under an inert atmosphere.

The exchange coupling of iron and copper ions via superexchange through bridging ligands[26] is usually described in the framework of the Heisenberg–Dirac–Van Vleck (HDVV) model, which takes into account only ground states of interacting ions. These ground states are formed by local crystal fields, and most cases are nondegenerate for transition metal ions. Because of the approximate nature of the HDVV model, it has limited applications for multielectron ions.[27]

For iron complexes, the consideration of either high-spin or low-spin isolated singlets is typically adequate to describe magnetochemical and spectroscopic data. However, it is now recognized that, in certain heme proteins, a quantum spin mixture of iron states must be taken into account.[28] In a local octahedral environment, the ground state of iron(III) is a $^6A_1$ orbital singlet and the first excited state is a $^4T_1$ orbital triplet. In ferric heme proteins in which there is only one strong axial ligand, the symmetry at the iron site is approximately C_{4v} and the first excited state will be split into ^4E and $^4A_2$ states. Depending upon the ratio of the crystal field parameter Δ and the spin–orbit coupling constant, the ground state may have spin $^3/_2$, and the ground and excited states may be strongly coupled by spin–orbit interactions. Thus, there will not be pure spin states $^3/_2$ or $^5/_2$, but the ground state will be an admixture that includes the orbital motion. The ^4E excited state lies very high in energy and will not be taken into account in this model.

The symmetric $^6A_1(t_2^3e^2)$ state corresponds to a $d^1_{xy}d^1_{xz}d^1_{yz}d^1_{z^2}d^1_{x^2-y^2}$ electronic configuration, while the $^4A_2(t_2^4e^1)$ state corresponds to the electronic configuration $d^2_{xy}d^1_{xz}d^1_{yz}d^1_{z^2}$. For subsequent applications the exact expressions for the wave functions of the quartet and sextet states were needed. These functions were designated as $|\Gamma_1(t_2^x)\gamma_1 S_1 M_1 \Gamma_2 (e^y)\gamma_2 S_2 M_2, \Gamma(t_2^x e^y)\gamma SM\rangle$, where $\Gamma\gamma$ are the irreducible representation and the corresponding row of the point group C_{4v} and SM are the total spin value and spin projection. These wave functions were constructed from the one-electron spin orbitals of the d-shell as described in detail by Sugano et al.[29] Following this procedure, one can obtain

$$|A(t_2^x e^y) S_{Fe} M\rangle = \sum_{\substack{\Gamma_1\gamma_1 S_1 M_1 \\ \Gamma_2\gamma_2 S_2 M_2}} \|\Gamma_1(t_2^x)\gamma_1 S_1 M_1\rangle|\Gamma_2(e^y)\gamma_2 S_2 M_2\rangle|\langle\Gamma_1\gamma_1\Gamma_2\gamma_2|A_1\rangle C^{S_{Fe}M}_{S_1 M_1 S_2 M_2} \quad (1)$$

where $\langle\ldots\ldots|\ldots\rangle$ are the Clebsch–Gordan coefficients with cubic bases,[29] $C^{\cdots}$ are the Wigner coefficients,[30,31] and $|\ldots|$ are Slater determinants. When the summation in eq 1 is carried out over all possible values of $M_1 M_2 \gamma_1 \gamma_2$ for each set of the representations Γ_1 and Γ_2, the resulting A representation (A_1 or A_2) is obtained. These wave functions are automatically antisymmetric with respect to the electron exchange, so they satisfy the Pauli principle. Since they are the bases of irreducible representations of the point group, they will diagonalize the crystal field Hamiltonian. At the same time these functions will be the eigenfunctions of S^2 and S_z with eigenvalues $S(S+1)$ and M, respectively (S equals $^5/_2$ or $^3/_2$ for the A_1 and A_2 orbital singlets).

From this procedure, the eigenfunctions of the iron ion are found to be

$$|A_1\,{}^5/_2, {}^5/_2\rangle = \frac{1}{\sqrt{5!}}|\xi\eta\zeta uv| \quad (2a)$$

$$|A_2\,{}^3/_2, {}^3/_2\rangle = \frac{1}{\sqrt{5!}}|\xi\eta\bar{\zeta}\zeta u| \quad (2b)$$

where $\xi = yz$, $\eta = xz$, $\zeta = xy$, $u = 3z^2 - r^2$, and $v = x^2 - y^2$ are one-electron spin–orbitals of the d-shell and $\bar{\zeta}$ is the spin–orbital ζ with negative projection of the electron spin ($-^1/_2$). The functions with the maximum spin projection are listed in eqs 2, and the rest can be obtained by successive operations of S_-.

Using the same procedure, the $^2A_1(t_2^6e^3)$ wave functions of the Cu^{2+} are generated as

$$|A_1\,{}^1/_2, {}^1/_2\rangle = \frac{1}{\sqrt{9!}}|\xi\bar{\xi}\eta\bar{\eta}\zeta\bar{\zeta}uv\bar{v}| \quad (3a)$$

$$|A_1\,{}^1/_2, {}^{-1}/_2\rangle = \frac{1}{\sqrt{9!}}|\xi\bar{\xi}\eta\bar{\eta}\zeta\bar{\zeta}\bar{u}v\bar{v}| \quad (3b)$$

When the quantum mixed state of the iron ion and the superexchange interaction between iron and copper are taken into account, the Hamiltonian becomes

$$\mathbf{H} = \mathbf{H}_{cr} + \mathbf{H}_{so} + \mathbf{H}_{exc} + \mathbf{H}_{zfs} + \mathbf{H}_{Z} \quad (4)$$

(18) Foner, S. *Rev. Sci. Instrum.* **1959**, *30*, 548.
(19) Losee, D. B.; Hatfield, W. E. *Phys. Rev. B: Solid State* **1974**, *10*, 212.
(20) Figgis, B. N.; Nyholm, R. S. *J. Chem. Soc.* **1958**, 4190.
(21) Brown, D. B.; Crawford, V. H.; Hall, J. W.; Hatfield, W. E. *J. Phys. Chem.* **1977**, *81*, 1303.
(22) Type TG-100 FPA (Special), No. 4277, Lake Shore Cryotronics, Westerville, OH.
(23) Konig, E. *Magnetic Properties of Transition Metal Compounds*; Springer-Verlag: West Berlin, 1966.
(24) Weller, R. R.; Hatfield, W. E. *J. Chem. Educ.* **1979**, *56*, 652.
(25) Eaton, G. R.; Eaton, S. S. *Inorg. Chem.* **1980**, *19*, 1095.
(26) Hatfield, W. E.; Elliott, C. M.; Ensling, J.; Akabori, K. *Inorg. Chem.* **1987**, *26*, 1930.
(27) Tsukerblat, B. S.; Belinskii, M. I.; Fainzilberg, V. E. *Sov. Sci. Rev., Sect. B, Chem. Rev.* **1987**, *9*, 337–481.
(28) Maltempo, M. M.; Moss, T. H. *Q. Rev. Bioph.* **1976**, *9*, 181.
(29) Sugano, S.; Tanabe, Y.; Kamimura, H. *Multiplets of Transition-Metal Ions in Crystals*; Academic Press: New York, 1970.
(30) Judd, B. R. *Operator Techniques in Atomic Spectroscopy*; McGraw-Hill: New York, 1963.
(31) Varshalovich, D. A.; Moskalev, A. N.; Ckersonskii, V. K. *Quantum Theory of Angular Momentum*; "Nauka": Leningrad, 1975 (Russian).

Table VI. Selected Bond Lengths (Å)[a] and Angles (deg)[a] for **2**

Cu–S1	2.308 (3)	C4–C5	1.391 (13)	N5–C74	1.373 (11)	N12–C66	1.171 (15)	Fe–O1	2.219 (7)	C81–C82	1.433 (13)
Cu–S2	2.227 (3)	C5–C6	1.407 (11)	N6–C76	1.372 (11)	S1–Fe	2.434 (3)	O1–C50	1.464 (15)	C82–C83	1.387 (11)
Cu–S3	2.245 (3)	C6–C7	1.466 (13)	N6–C79	1.363 (12)	Fe–N1	2.031 (7)	O1–C53	1.432 (12)	C83–C84	1.453 (13)
Cu–S4	2.287 (3)	C7–C8	1.342 (11)	N7–C81	1.387 (12)	Fe–N2	2.001 (8)	C50–C51	1.470 (19)	C84–C85	1.403 (12)
S1–C67	1.774 (10)	C8–C9	1.433 (14)	N7–C84	1.387 (11)	Fe–N3	1.987 (6)	C51–C52	1.477 (20)	C85–C86	1.382 (14)
S2–C60	1.726 (9)	C9–C10	1.405 (12)	N8–C86	1.385 (11)	Fe–N4	1.995 (8)	C52–C53	1.478 (18)	C86–C87	1.424 (12)
S3–C62	1.726 (9)	C10–C11	1.392 (14)	N8–C89	1.409 (12)	N1–C1	1.391 (11)	O2–C120	1.443 (12)	C87–C88	1.371 (14)
S4–C64	1.709 (11)	C11–C12	1.445 (11)	C71–C72	1.435 (14)	N1–C4	1.381 (13)	O2–C123	1.436 (14)	C88–C89	1.400 (11)
C60–C61	1.454 (13)	C12–C13	1.351 (14)	C72–C73	1.342 (13)	N2–C6	1.384 (11)	C120–C121	1.501 (17)	C89–C90	1.378 (13)
C60–C62	1.384 (13)	C13–C14	1.463 (12)	C73–C74	1.454 (15)	N2–C9	1.382 (11)	C121–C122	1.519 (21)	C71–C90	1.415 (11)
C62–C63	1.476 (13)	C14–C15	1.398 (13)	C74–C75	1.416 (12)	N3–C11	1.398 (11)	C122–C123	1.481 (15)	Ga–O3	2.113 (7)
N9–C61	1.129 (13)	C15–C16	1.381 (11)	C75–C76	1.407 (14)	N3–C14	1.360 (12)	O2–Ga	2.152 (7)	O3–C130	1.459 (12)
N10–C63	1.099 (14)	C16–C17	1.412 (13)	C76–C77	1.448 (12)	N4–C16	1.379 (12)	Ga–N5	2.031 (8)	O3–C133	1.387 (14)
C64–C65	1.355 (16)	C17–C18	1.375 (11)	C77–C78	1.346 (14)	N4–C19	1.367 (11)	Ga–N6	2.003 (7)	C130–C131	1.463 (17)
C64–C67	1.383 (16)	C18–C19	1.473 (13)	C78–C79	1.429 (11)	C1–C2	1.409 (13)	Ga–N7	2.005 (8)	C131–C132	1.520 (24)
C66–C67	1.426 (14)	C19–C20	1.406 (12)	C79–C80	1.404 (14)	C2–C3	1.363 (14)	Ga–N8	2.036 (7)	C132–C133	1.444 (22)
N11–C65	1.203 (15)	C1–C20	1.369 (14)	C80–C81	1.375 (12)	C3–C4	1.441 (12)	N5–C71	1.390 (12)		

S1–Cu–S2	87.7 (1)	S1–Cu–S3	177.2 (1)	O1–Fe–N2	90.1 (3)	O1–Fe–N3	89.7 (3)
S1–Cu–S4	89.2 (1)	S2–Cu–S3	92.1 (1)	O1–Fe–N4	85.7 (3)	Fe–O1–C50	124.1 (6)
S2–Cu–S4	174.0 (1)	S3–Cu–S4	91.2 (1)	Fe–O1–C53	124.2 (7)	O1–C50–C51	105.8 (9)
Cu–S1–C67	99.7 (4)	Cu–S2–C60	99.7 (3)	O1–C53–C52	107.9 (9)	C50–O1–C53	109.3 (8)
Cu–S3–C62	100.6 (3)	Cu–S4–C64	102.8 (5)	C50–C51–C52	107.1 (13)	C51–C52–C53	105.5 (10)
S2–C60–C61	117.2 (7)	S2–C60–C62	123.6 (6)	O2–C120–C121	106.8 (9)	O2–C123–C122	108.3 (9)
S3–C62–C60	120.7 (6)	S3–C62–C63	118.3 (7)	C120–O2–C123	109.1 (8)	C120–C121–C122	104.1 (10)
C60–C62–C63	120.9 (8)	C60–C61–N9	176.0 (11)	C121–C122–C123	103.8 (12)	C120–O2–Ga	126.8 (7)
C61–C60–C62	119.1 (8)	C62–C63–N10	172.3 (14)	C123–O2–Ga	122.6 (5)	O2–Ga–N5	87.9 (3)
S1–C67–C64	122.0 (8)	S1–C67–C66	116.0 (8)	O2–Ga–N6	88.7 (3)	O2–Ga–N7	90.1 (3)
S4–C64–C67	121.8 (9)	S4–C64–C65	119.3 (9)	O2–Ga–N8	90.6 (3)	N5–Ga–N6	90.3 (3)
C64–C65–N11	175.1 (15)	C64–C67–C66	122.0 (9)	N5–Ga–N7	177.6 (3)	N5–Ga–N8	88.9 (3)
C65–C64–C67	118.9 (10)	C67–C66–N12	178.1 (12)	N6–Ga–N7	91.0 (3)	N6–Ga–N8	178.9 (3)
Cu–S1–Fe	112.3 (1)	C67–S1–Fe	106.3 (4)	N7–Ga–N8	89.9 (3)	Ga–N5–C71	128.2 (6)
S1–Fe–O1	173.0 (2)	S1–Fe–N1	92.7 (2)	Ga–N5–C74	126.7 (6)	Ga–N6–C86	126.5 (6)
S1–Fe–N2	96.7 (2)	S1–Fe–N3	91.9 (2)	Ga–N6–C89	126.6 (6)	Ga–N7–C81	125.8 (6)
S1–Fe–N4	87.4 (2)	N1–Fe–N2	88.8 (3)	Ga–N7–C84	126.6 (6)	Ga–N8–C76	127.5 (7)
N1–Fe–N3	175.4 (3)	N1–Fe–N4	91.0 (3)	Ga–N8–C79	127.4 (6)	C71–N5–C74	105.0 (8)
N2–Fe–N3	90.1 (3)	N2–Fe–N4	175.8 (3)	N5–C71–C72	109.7 (7)	N5–C71–C90	125.4 (9)
N3–Fe–N4	89.8 (3)	Fe–N1–C1	125.3 (6)	C71–C72–C73	108.5 (10)	C72–C73–C74	105.8 (9)
Fe–N1–C4	128.1 (6)	Fe–N2–C6	127.2 (5)	N5–C74–C73	111.0 (7)	N5–C74–C75	126.3 (9)
Fe–N2–C9	128.0 (6)	Fe–N3–C11	126.6 (6)	C73–C74–C75	122.6 (8)	C74–C75–C76	122.2 (8)
Fe–N3–C14	126.3 (6)	Fe–N4–C16	128.3 (6)	C76–N6–C79	106.8 (7)	N6–C76–C75	127.7 (8)
Fe–N4–C19	125.5 (6)	C1–N1–C4	106.4 (7)	N6–C76–C77	108.8 (8)	C75–C76–C77	123.5 (8)
N1–C1–C2	108.8 (8)	N1–C1–C20	126.7 (8)	C76–C77–C78	107.2 (7)	C77–C78–C79	107.2 (8)
C1–C2–C3	109.2 (8)	C2–C3–C4	105.8 (8)	N6–C79–C78	110.0 (8)	N6–C79–C80	125.4 (7)
N1–C4–C3	109.7 (8)	N1–C4–C5	126.1 (7)	C78–C79–C80	124.6 (8)	C79–C80–C81	125.3 (9)
C3–C4–C5	124.2 (8)	C4–C5–C6	121.9 (8)	C81–N7–C84	106.8 (7)	N7–C81–C80	125.5 (9)
C6–N2–C9	104.4 (7)	N2–C6–C5	127.4 (8)	N7–C81–C82	110.0 (7)	C80–C81–C82	124.4 (8)
N2–C6–C7	110.3 (7)	C5–C6–C7	122.2 (8)	C81–C82–C83	107.1 (8)	C82–C83–C84	106.7 (8)
C6–C7–C8	106.2 (8)	C7–C8–C9	107.6 (8)	N7–C84–C83	109.3 (7)	N7–C84–C85	126.0 (9)
N2–C9–C8	111.2 (7)	N2–C9–C10	125.0 (9)	C83–C84–C85	124.6 (8)	C84–C85–C86	125.1 (8)
C8–C9–C10	123.7 (8)	C9–C10–C11	123.1 (8)	C86–N8–C89	105.1 (7)	N8–C86–C85	124.7 (7)
C11–N3–C14	107.1 (7)	N3–C11–C10	126.8 (8)	N8–C86–C87	110.0 (8)	C85–C86–C87	125.3 (8)
N3–C11–C12	108.5 (8)	C10–C11–C12	124.6 (8)	C86–C87–C88	107.1 (7)	C87–C88–C89	107.9 (8)
C11–C12–C13	107.9 (7)	C12–C13–C14	106.7 (8)	N8–C89–C88	109.9 (8)	N8–C89–C90	126.1 (7)
N3–C14–C13	109.6 (8)	N3–C14–C15	127.8 (7)	C88–C89–C90	124.0 (8)	C89–C90–C71	124.1 (8)
C13–C14–C15	122.6 (8)	C14–C15–C16	123.0 (8)	C90–C71–C72	124.9 (9)	N5–Ga–O3	92.0 (3)
C16–N4–C19	106.2 (8)	N4–C16–C15	124.5 (9)	N6–Ga–O3	89.6 (3)	N7–Ga–O3	90.0 (3)
N4–C16–C17	110.9 (7)	C15–C16–C17	124.5 (8)	N8–Ga–O3	91.1 (3)	O2–Ga–O3	178.3 (3)
C16–C17–C18	107.8 (8)	C17–C18–C19	105.2 (7)	Ga–O3–C130	124.3 (6)	Ga–O3–C133	123.9 (7)
N4–C19–C18	109.9 (7)	N4–C19–C20	128.1 (9)	O3–C130–C131	107.8 (9)	O3–C133–C132	110.4 (12)
C18–C19–C20	122.0 (7)	C19–C20–C1	123.1 (8)	C130–03–C133	106.0 (7)	C130–C131–C132	105.6 (11)
C20–C1–C2	124.4 (8)	O1–Fe–N1	85.9 (3)	C131–C132–C133	102.3 (14)		

[a] Estimated standard deviations in the least significant digits are given in parentheses.

where $\mathbf{H}_{cr}$ ($=\Delta\sigma_z$) is the Hamiltonian of the C_{4v} crystal field at the iron site, which represents the energy gap Δ between the two iron orbital singlet states. The Hamiltonian was written in terms of Pauli matrices in the bases $^6A_1$ and $^4A_2$, respectively. $\mathbf{H}_{so}$ ($=\lambda\mathbf{LS}$) is the spin–orbit interaction which mixes the iron states; $\mathbf{H}_{exc}$ ($=-2J\mathbf{S}_{Fe}\mathbf{S}_{Cu}$) is the HDVV isotropic exchange interaction; $\mathbf{H}_{zfs}$ is the zero-field splitting term, which will be discussed below; and $\mathbf{H}_Z$ ($=g_{Fe}\mu_B\mathbf{BS}_{Fe} + g_{Cu}\mu_B\mathbf{BS}_{Cu}$) represents the interaction with the external magnetic field B. This interaction is assumed to be isotropic. The quantities g_{Fe}, g_{Cu}, and μ_B are electron g-factors and the Bohr magneton, respectively.

Since the Hamiltonian in (4) includes an isotropic exchange term, the question arises whether the interaction of copper with the two iron orbital singlet states can be described in terms of one exchange parameter, J. Generally speaking, it is not immediately obvious that the Heisenberg model will hold true for the description of the exchange interaction of copper with two iron orbital singlet states simultaneously.

To find a solution to this problem, it is necessary to derive the wave functions of the total spin in a scheme which involves addition of the copper moment with the two iron moments. Although these functions consist of the same spin–orbitals, they are not orthogonal because they belong to the different sites of the cluster. According to the procedure presented above, these functions are obtained in the following form by using eqs 2 and 3:

$$|S(S_{Fe},S_{Cu})M\rangle = f_n \sum_{M_{Fe}M_{Cu}} \|S_{Fe}M_{Fe}\rangle|S_{Cu}M_{Cu}\rangle|C^{SM}_{S_{Fe}M_{Fe}S_{Cu}M_{Cu}} \quad (5)$$

Here f_n is the normalization factor, including the overlap integrals of the

Table VII. Selected Bond Lengths (Å)[a] and Angles (deg)[a] for **3**

Cu–S1	2.283 (3)	C2–C3	1.349 (12)	Al–N6	1.997 (7)	N9–C63	1.056 (14)	C18–C19	1.444 (12)	C76–C77	1.448 (13)
Cu–S2	2.259 (4)	C3–C4	1.441 (14)	Al–N7	1.991 (8)	N10–C62	1.065 (13)	C19–C20	1.370 (13)	C77–C78	1.340 (12)
Cu–S3	2.266 (3)	C4–C5	1.379 (12)	Al–N8	1.999 (7)	S1–Fe	2.444 (3)	C1–C20	1.382 (11)	C78–C79	1.425 (14)
Cu–S4	2.240 (3)	C5–C6	1.410 (14)	N5–C76	1.355 (11)	Fe–N1	1.998 (8)	Fe–O1	2.255 (7)	C79–C80	1.393 (13)
S1–C66	1.741 (10)	C6–C7	1.445 (13)	N5–C79	1.371 (11)	Fe–N2	2.004 (7)	O1–C50	1.441 (13)	C80–C81	1.380 (14)
S2–C64	1.711 (12)	C7–C8	1.359 (16)	N6–C71	1.359 (11)	Fe–N3	2.018 (8)	O1–C53	1.440 (18)	C81–C82	1.397 (12)
S3–C61	1.698 (10)	C8–C9	1.416 (11)	N6–C74	1.408 (11)	Fe–N4	2.003 (7)	C50–C51	1.450 (19)	C82–C83	1.371 (15)
S4–C63	1.738 (10)	C9–C10	1.454 (13)	N7–C86	1.366 (12)	N1–C1	1.392 (11)	C51–C52	1.517 (23)	C83–C84	1.419 (12)
C64–C65	1.417 (16)	C10–C11	1.366 (12)	N7–C89	1.417 (11)	N1–C4	1.363 (11)	C52–C53	1.415 (20)	C84–C85	1.394 (15)
C64–C66	1.302 (16)	C11–C12	1.426 (15)	N8–C81	1.386 (12)	N2–C6	1.372 (12)	O3–C130	1.480 (11)	C85–C86	1.386 (12)
C66–C67	1.463 (16)	C12–C13	1.362 (13)	N8–C84	1.402 (12)	N2–C9	1.349 (12)	O3–C133	1.426 (14)	C86–C87	1.443 (14)
N11–C67	1.140 (17)	C13–C14	1.449 (14)	C71–C72	1.444 (12)	N3–C11	1.401 (11)	C130–C131	1.508 (16)	C87–C88	1.355 (13)
N12–C65	1.216 (18)	C14–C15	1.397 (11)	C72–C73	1.327 (14)	N3–C14	1.394 (11)	C131–C132	1.544 (20)	C88–C89	1.435 (14)
C60–C61	1.400 (15)	C15–C16	1.420 (14)	C73–C74	1.459 (12)	N4–C16	1.343 (12)	C132–C133	1.431 (16)	C89–C90	1.371 (13)
C60–C63	1.508 (13)	C16–C17	1.462 (12)	C74–C75	1.350 (13)	N4–C19	1.405 (12)	O2–Al	2.069 (7)	C71–C90	1.380 (14)
C61–C62	1.486 (13)	C17–C18	1.297 (14)	C75–C76	1.425 (11)	C1–C2	1.428 (14)	Al–N5	2.006 (9)	Al–O2	1.912 (8)

S1–Cu–S2	90.0 (1)	S1–Cu–S3	174.1 (1)	C18–C19–C20	126.4 (8)	C19–C20–C1	124.7 (8)
S1–Cu–S4	87.8 (1)	S2–Cu–S3	91.3 (1)	C20–C1–C2	125.8 (8)	O1–Fe–N2	86.7 (3)
S2–Cu–S4	174.0 (2)	S3–Cu–S4	91.4 (1)	O1–Fe–N3	90.0 (3)	O1–Fe–N4	87.8 (3)
Cu–S1–C66	99.5 (4)	Cu–S2–C64	99.5 (4)	Fe–O1–C50	124.5 (7)	Fe–O1–C53	125.8 (7)
Cu–S3–C61	101.3 (4)	Cu–S4–C60	101.0 (4)	O1–C50–C51	107.6 (10)	O1–C53–C52	110.0 (12)
S1–C66–C67	114.2 (8)	S1–C66–C64	121.6 (8)	C50–O1–C53	108.7 (9)	C50–C51–C52	107.0 (11)
S2–C64–C65	115.3 (10)	S2–C64–C66	125.6 (8)	C51–C52–C53	106.1 (4)	O3–C130–C131	105.2 (8)
C65–C64–C66	119.0 (11)	C66–C67–N11	175.6 (16)	O3–C133–C132	109.9 (9)	C130–O3–C133	108.2 (7)
C64–C66–C67	123.9 (10)	C64–C65–N12	178.6 (19)	C130–C131–C132	102.5 (9)	C131–C132–C133	104.3 (12)
S3–C61–C60	122.5 (8)	S3–C61–C62	119.9 (8)	C130–O3–Al	125.3 (6)	C133–O3–Al	125.7 (6)
S4–C60–C61	121.6 (7)	S4–C60–C63	116.8 (7)	O3–Al–N5	89.4 (3)	O3–Al–N6	88.2 (3)
C60–C63–N9	173.9 (12)	C61–C60–C63	121.5 (8)	O3–Al–N7	87.0 (3)	O3–Al–N8	89.7 (3)
C60–C61–C62	117.6 (8)	C61–C62–N10	176.3 (12)	N5–Al–N6	89.8 (3)	N5–Al–N7	176.3 (3)
Cu–S1–Fe	115.1 (1)	C66–S1–Fe	105.3 (4)	N5–Al–N8	89.7 (3)	N6–Al–N7	90.7 (3)
S1–Fe–O1	173.2 (2)	S1–Fe–N1	88.5 (2)	N6–Al–N8	177.8 (3)	N7–Al–N8	89.6 (3)
S1–Fe–N2	94.5 (2)	S1–Fe–N3	96.6 (2)	Al–N5–C76	126.4 (6)	Al–N5–C79	126.8 (6)
S1–Fe–N4	91.2 (2)	N1–Fe–N2	91.1 (3)	Al–N6–C71	126.7 (6)	Al–N6–C74	126.5 (6)
N1–Fe–N3	174.8 (3)	N1–Fe–N4	90.3 (3)	Al–N7–C86	128.7 (6)	Al–N7–C89	125.9 (6)
N2–Fe–N3	88.8 (3)	N2–Fe–N4	174.2 (3)	Al–N8–C81	128.2 (6)	Al–N8–C84	126.9 (6)
N3–Fe–N4	89.3 (3)	Fe–N1–C1	127.1 (6)	C71–N6–C74	106.8 (7)	N6–C71–C72	109.7 (8)
Fe–N1–C4	126.0 (6)	Fe–N2–C6	126.0 (6)	N6–C71–C90	126.7 (8)	C71–C72–C73	108.0 (8)
Fe–N2–C9	129.4 (6)	Fe–N3–C11	127.7 (6)	C72–C73–C74	107.9 (8)	N6–C74–C73	107.6 (8)
Fe–N3–C14	126.2 (6)	Fe–N4–C16	128.4 (6)	N6–C74–C75	127.6 (7)	C73–C74–C75	124.9 (8)
Fe–N4–C19	125.6 (6)	C1–N1–C4	106.6 (8)	C74–C75–C76	121.4 (8)	C76–N5–C79	106.1 (8)
N1–C1–C2	108.9 (7)	N1–C1–C20	124.9 (9)	N5–C76–C75	127.9 (8)	N5–C76–C77	110.1 (7)
C1–C2–C3	107.7 (8)	C2–C3–C4	107.1 (8)	C75–C76–C77	122.0 (8)	C76–C77–C78	106.3 (9)
N1–C4–C3	109.5 (7)	N1–C4–C5	127.0 (9)	C77–C78–C79	107.6 (9)	N5–C79–C78	109.9 (8)
C3–C4–C5	123.5 (8)	C4–C5–C6	123.8 (8)	N5–C79–C80	125.5 (9)	C78–C79–C80	124.6 (8)
C6–N2–C9	104.5 (7)	N2–C6–C5	125.8 (7)	C79–C80–C81	125.5 (8)	C81–N8–C84	105.0 (7)
N2–C6–C7	110.2 (9)	C5–C6–C7	123.9 (9)	N8–C81–C80	124.0 (7)	N8–C81–C82	109.6 (8)
C6–C7–C8	106.6 (9)	C7–C8–C9	105.6 (9)	C80–C81–C82	126.5 (8)	C81–C82–C83	109.6 (8)
N2–C9–C8	113.0 (8)	N2–C9–C10	124.4 (7)	C82–C83–C84	105.2 (8)	N8–C84–C83	110.7 (9)
C8–C9–C10	122.5 (8)	C9–C10–C11	124.0 (9)	N8–C84–C85	125.3 (8)	C83–C84–C85	124.0 (8)
C11–N3–C14	105.2 (8)	N3–C11–C10	124.7 (9)	C84–C85–C86	124.2 (9)	C86–N7–C89	105.3 (8)
N3–C11–C12	109.7 (8)	C10–C11–C12	125.5 (9)	N7–C86–C85	125.1 (9)	N7–C86–C87	110.7 (7)
C11–C12–C13	108.1 (9)	C12–C13–C14	108.2 (9)	C85–C86–C87	124.1 (9)	C86–C87–C88	107.1 (9)
N3–C14–C13	108.8 (7)	N3–C14–C15	127.2 (8)	C87–C88–C89	107.6 (9)	N7–C89–C88	109.3 (7)
C13–C14–C15	124.0 (8)	C14–C15–C16	121.1 (8)	N7–C89–C90	125.3 (9)	C88–C89–C90	125.5 (8)
C16–N4–C19	105.9 (7)	N4–C16–C15	127.3 (8)	C89–C90–C71	124.6 (8)	C90–C71–C72	123.6 (8)
N4–C16–C17	111.0 (8)	C15–C16–C17	121.6 (8)	N5–Al–O2	93.7 (3)	N6–Al–O2	91.7 (3)
C16–C17–C18	105.5 (8)	C17–C18–C19	110.5 (8)	N7–Al–O2	89.9 (3)	N8–Al–O2	90.5 (3)
N4–C19–C18	107.0 (8)	N4–C19–C20	126.6 (7)	O2–Al–O3	176.9 (3)		

[a] Estimated standard deviations in the least significant digits are given in parentheses.

nonorthogonal one-electron spin–orbitals at different sites. It follows from (5) that there are 20 wave functions of the total spin, these being $|3(^5/_2,^1/_2)M\rangle$, $|2(^5/_2,^1/_2)M\rangle$, $|2(^3/_2,^1/_2)M\rangle$, and $|1(^3/_2,^1/_2)M\rangle$. The resultant diagonalization of the Coulomb interaction of the multielectron dinuclear anion on the bases of functions (5) gives the expressions for the eigenvalues, including Coulomb, exchange, and overlap integrals (see the similar procedure used by Tsukerblat et al.[27]). When these eigenvalues are expanded in a power series and only second-order terms with respect to overlap integrals are retained, it may be seen that the exchange interaction of copper with the two iron singlets is expressed in terms of the same exchange parameter J and that all nondiagonal terms of the exchange matrix vanish.

Thus, in the frame of the present approximation (the same approximation which is used for derivation of the Heisenberg multielectron exchange interaction) the functions (5) are the eigenfunctions of the HDVV exchange Hamiltonian.

The fourth term (zero field splitting) of the Hamiltonian (4) takes the form $\mathbf{H}_{zfs} = D[\mathbf{S}_z^2 - {}^1/_3 S(S+1)]$ and acts on the bases of the total spin functions (5).

The diagonalization of the 20 × 20 matrix (4) in the bases (5) was carried out on an IBM 3090. The eigenvalues were used to calculate the temperature dependence of the magnetic moment and the magnetic susceptibility.

Magnetization and magnetic susceptibility (per one atom) were determined by the standard thermodynamic relations in eqs 6, where α,

$$\mu_\alpha = kT\frac{\partial \ln (Z)}{\partial B_\alpha} \tag{6a}$$

$$\chi_{\alpha\beta} = kT\frac{\partial \ln (Z)}{\partial B_\alpha \partial B_\beta} \tag{6b}$$

Table VIII. Mössbauer Parameters

	1 (site a)	1 (site b)	2	3
isomer shift, δ (mm/s)	0.40	0.36	0.36	0.37
quadrupole splitting, ΔE (mm/s)	2.66	2.55	2.64	2.61
line width, Γ (mm/s)	0.40	0.40	0.38	0.38
asym param, η	0.37	0.38		
Spin Hamiltonian Parameters for Site a				
electronic	$D = 15.3$ cm^{-1}, $E/D = 0$			
magnetic hyperfine (excited state)	$A_{xx}/g_n\beta_n = -27.8$ T, $A_{yy}/g_n\beta_n = -27.8$ T, $A_{zz}/g_n\beta_n = +7.4$ T[a]			
Spin Hamiltonian Parameters for Site b				
electronic	$g_{xx} = 1.8$, $g_{yy} = 1.8$, $g_{zz} = 2.0$			
magnetic hyperfine field	$H_x = -12.3$ T, $H_y = -12.2$ T, $H_z = -0.3$ T in 6 T applied field[a]			
	$H_x = -18.0$ T, $H_y = -15.4$ T, $H_z = -0.3$ T in 8 T applied field[a]			

[a] Negative magnetic hyperfine fields oppose the applied field.

$\beta = x, y, z$, $Z = \sum_{i=1}^{20} \exp(-E_i/kT)$ (E_i values are energy levels of the Hamiltonian (4)) is the partition function of the system interacting with the external magnetic field B, and μ_α and $\chi_{\alpha\beta}$ are the components of the magnetization vector and the magnetic susceptibility tensor, respectively. Since the system under consideration possesses axial symmetry, the magnetic susceptibility will depend only upon the orientation of the magnetic field with respect to the local symmetry axis. Thus, the final expressions for magnetization per atom and magnetic susceptibility of a powdered sample are

$$M = \frac{2}{\pi}\int_0^{\pi} \mu_\alpha \sin^2\theta \, d\theta \tag{7a}$$

$$\chi = \frac{2}{\pi}\int_0^{\pi} \chi_{\alpha\beta} \sin^2\theta \, d\theta \tag{7b}$$

Here θ is the angle between the external magnetic field and the local symmetry axis.

Equations 7a and 7b are the complete expressions used for the calculation of the magnetization and magnetic suceptibility for compounds **2** and **3**. The presence of an additional iron(III) ion in **1** provided additional complications in terms of modeling of its magnetic behavior; thus, only the simpler cases of compounds **2** and **3** are reported here.

Mössbauer Spectroscopy. Mössbauer spectra for **1–3** were determined using a constant-acceleration spectrometer equipped with a ^{57}Co source in a Rh matrix. The samples are the same as those used for the magnetic susceptibility measurements. Mössbauer spectra in zero applied field were taken in horizontal transmission geometry with the source at room temperature. Spectra in applied fields of 6 and 8 T were taken in vertical transmission geometry with the source and absorber at 4.2 K. The isomer shifts reported are with respect to the centroid of the spectrum of metallic Fe at room temperature. The line widths obtained from the calibration spectra were typically 0.28 mm/s.

Initial attempts to fit the spectra of **1** with a single-site model were fruitless. In view of the crystallographic information, a two-site calculation was required in which each site contributed equally to the spectrum. For each site, the electronic part of the Hamiltonian was solved first to yield spin expectation values for a given direction of the applied field. The components of the magnetic hyperfine field at the nucleus were assumed to be proportional to the spin expectation values, the constants of proportionality being A_{ii}. A powder spectrum was simulated by placing the applied field in equal increments of solid angle over an octant of the unit sphere. A 10 × 10 grid was used for the simulations shown (Figures 9 and 10).

The electronic part of the Hamiltonian for site a was treated with an axial spin Hamiltonian

$$\mathbf{H} = D[S_z^2 - S(S+1)/3] + 2g\mu_B\mathbf{B}\cdot\mathbf{S} \tag{8}$$

with $S = {}^3/_2$. The variable parameters in the calculation were the quadrupole splitting parameter, the asymmetry parameter (η), D, and the axial magnetic hyperfine tensor (A_{xx}, A_{yy}, A_{zz}).

The electronic part for site b was treated with a phenomenological spin Hamiltonian

$$\mathbf{H}_Z = g_{xx}\mu_B B_x S_x + g_{yy}\mu_B B_y S_y + g_{zz}\mu_B B_z S_z \tag{9}$$

with effective spin $S = {}^1/_2$. The variable parameters in the calculation were the quadrupole splitting parameter, the asymmetry parameter, the values of g_{ii}, and the three components of the magnetic hyperfine tensor.

The data for **2** and **3** were fit by a least-squares method to obtain the parameters. Table VIII contains the parameters that provided the best fit to the data.

EPR Spectroscopy. The solid and frozen-solution EPR spectra of **1–3** were obtained on an IBM ER200 spectrometer equipped with an Oxford ESR900 liquid-helium cryostat. Quantitation of the signals was based on double integration of the spectra using [Fe(TPP)(O_3SCF_3)] and $(TBA)_2$[Cu(MNT)$_2$] as standards. Compound **1** exhibited a spectrum best assigned as arising solely from the [Fe^{III}(TPP)(THF)$_2$]$^+$ cation,[11] while compounds **2** and **3** exhibit very weak iron(III) EPR signals in the solid state at 5 K that are best attributed to a low level of disorder involving substitution of Ga(III) or Al(III) in the cation by Fe(III).

To interpret the absence of EPR spectra for **2** and **3**, the energy levels as a function of magnetic field were calculated for the Hamiltonian shown in eq 10,[32] where the subscripts 1 and 2 refer to the Fe(III) and Cu(II)

$$\mathbf{H} = -2J\mathbf{S}_1\cdot\mathbf{S}_2 + D[S_{1z}^2 - {}^1/_3 S_1(S_1+1)] + \mathbf{H}_{dip} + g_1\mu_B\mathbf{B}\cdot\mathbf{S}_1 + g_2\mu_B\mathbf{B}\cdot\mathbf{S}_2 \tag{10}$$

spins, respectively. This Hamiltonian differs from the implementation of eq 4 that was used to analyze the magnetic susceptibility data in that the zero field splitting (ZFS) term (D) acts on the spin functions for Fe(III) rather than the total spin functions.

The value of D obtained from the magnetic susceptibility data is intermediate between the values for the $S = 2$ and $S = 3$ states. Similarly, the value of D in eq 10 is intermediate between the values for the $S = 2$ and $S = 3$ states. As discussed below, the absence of EPR signals for Fe(III)–Cu(II) spin-coupled compounds is predicted for a range of values of D. The differences in the definition of D in the two Hamiltonians employed herein are not great enough to alter the conclusions. Values of J, D, g_{Fe} (g_1), and g_{Cu} (g_2) were taken from Table X. The interspin distance, r, was taken to be roughly 4.0 Å from the results of the X-ray crystallographic study. The z axis for the Fe(III) ZFS was assumed to coincide with the normal to the porphyrin plane, and a 30° angle (θ) between the interspin vector and the z axis for the Fe(III) ZFS was estimated. Since the dipolar interaction is much smaller than the exchange and ZFS terms, the calculated energy levels were insensitive to changes in r and θ. Energy levels were calculated by diagonalization of the energy matrix at 100-G intervals from 0 to 15 000 G.

A representative plot is shown in Figure 12, in which energies are given on a relative scale with average energy = 0.0. Energy levels are designated by labels that apply only in the limit of $J \gg D$. Transition probabilities were calculated for the conventional EPR geometry in which the microwave magnetic field, B_1, is perpendicular to the external magnetic field, B_0.

Table IX. Comparison of the Dinuclear Fe^{III}/Cu^{II} Anions

	1 (20 °C)	1 (−130 °C)	2	3
Fe1–Np (Å)	2.01 (1)	2.00 (1)	2.00 (2)	2.006 (9)
Fe1–S1 (Å)	2.549 (4)	2.411 (3)	2.434 (3)	2.444 (3)
Fe1–S–Cu (deg)	113.4 (1)	112.5 (1)	112.3 (1)	115.1 (1)
Cu–S1 (Å)	2.300 (4)	2.307 (3)	2.308 (3)	2.283 (3)
Cu–S_{av} (Å)	2.26 (4)	2.26 (3)	2.27 (4)	2.26 (2)
Fe1–O1 (Å)	2.346 (9)	2.212 (7)	2.219 (7)	2.255 (7)
Fe1–Ct_N (Å)	0.11	0.08	0.08	0.09
Fe1···Cu (Å)	4.056 (5)	3.924 (4)	3.938 (4)	3.989 (4)

Table X. Magnetic Susceptibility Best-Fit Theoretical Parameters

	Δ (cm^{-1})	λ (cm^{-1})	D (cm^{-1})	J (cm^{-1})	g_{Fe}	g_{Cu}	10^4R
2	2656.2	286.59	13.28	−17.94	1.98	2.16	5.936
3	2796.0	253.92	4.83	−15.18	1.98	2.20	2.019

Results and Discussion

Crystal Structures. The structures of **1–3** are shown in Figures 1–3. All three compounds contain a dinuclear anion consisting of an iron(III) porphyrin that is bound through a bridging sulfur atom to the copper(II) atom of a [Cu(MNT)$_2$]$^{2-}$ anion. The sixth coordination site about the iron atom of the anion is occupied

(32) More, K. M.; Eaton, G. R.; Eaton, S. S.; Hideg, K. *Inorg. Chem.* **1986**, *25*, 3865.

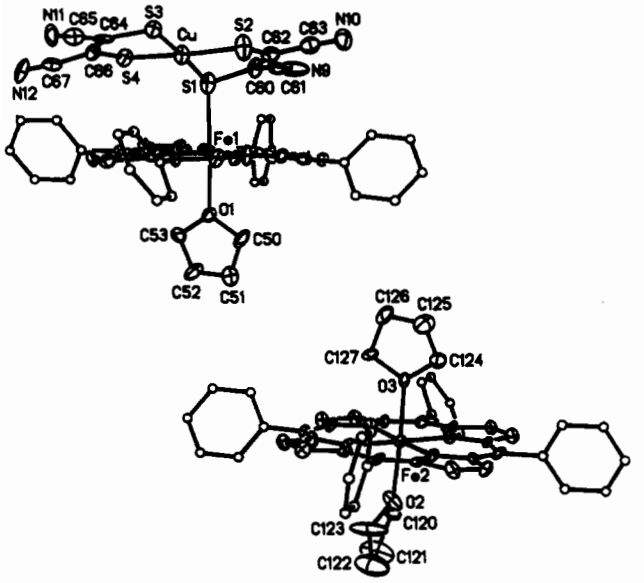

Figure 1. View of **1** at −130 °C. Thermal ellipsoids are drawn at the 50% probability level, carbon atoms of the phenyl rings have been drawn as spheres of arbitrary radius for clarity, and hydrogen atoms have been omitted. The numbering schemes for the THF and MNT^{2-} ligands are shown.

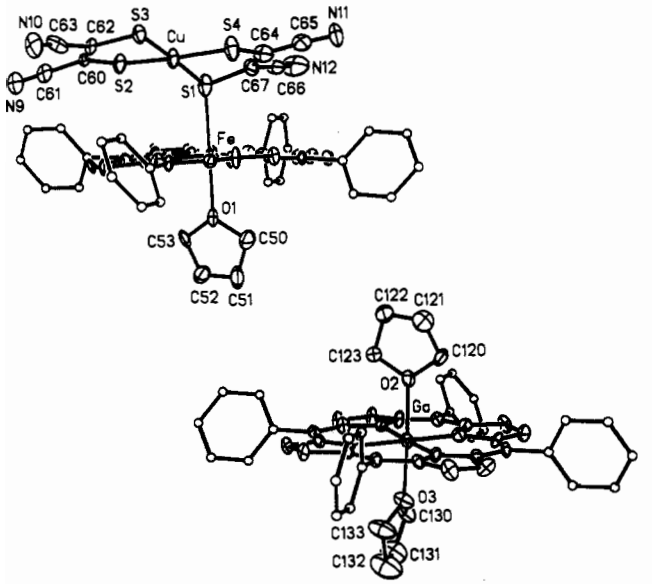

Figure 2. View of **2**. Thermal ellipsoids are drawn at the 50% probability level, carbon atoms of the phenyl rings have been drawn as spheres of arbitrary radius for clarity, and the hydrogen atoms have been omitted. The numbering schemes for the THF and MNT^{2-} ligands are shown.

in each case by a THF molecule. The cation in all three compounds is a M(III) porphyrin, where M = Fe in **1**, Ga in **2**, and Al in **3**. Figures 4–6 show the numbering scheme employed for the porphyrin ligands in each case and the deviations from the best least-squares plane through the 24 atoms of each porphyrin core.

The assignment of the copper oxidation states is clear-cut from the metric parameters. For $[Cu(MNT)_2]^{2-}$, Cu(II)–S(av) = 2.28 (2) Å,[33] which is similar to the values for Cu–S(av) in **1** (2.26 (4) Å at 20 °C, 2.26 (3) Å at −130 °C), **2** (2.27 (4) Å), and **3** (2.26 (2) Å), whereas Cu(III)–S = 2.170 (8) Å in $[Cu(MNT)_2]^-$.[34] (Note that for all averages given, the number in parentheses is the standard deviation of the sample.) The bridging interaction results in each case in a tetrahedral distortion of the $[Cu^{II}(MNT)_2]^{2-}$ anion and a long Cu–S(bridging) distance. This is most evident in the room temperature structure of **1**, where Cu–S(bridging) = 2.300 (4) Å, Cu–S(nonbridging, av) = 2.25 (3) Å, and the deviations of the sulfur atoms from the best least-squares plane through copper and the four surrounding sulfur atoms are +0.13, −0.12, +0.12, and −0.13 Å (for S1–S4, respectively). The other structures show similar distortions, but the magnitude of the distortions is smaller in the low-temperature structures (±0.09 Å for **1** at −130 °C, ±0.08 Å for **2**, and ±0.11 Å for **3**).

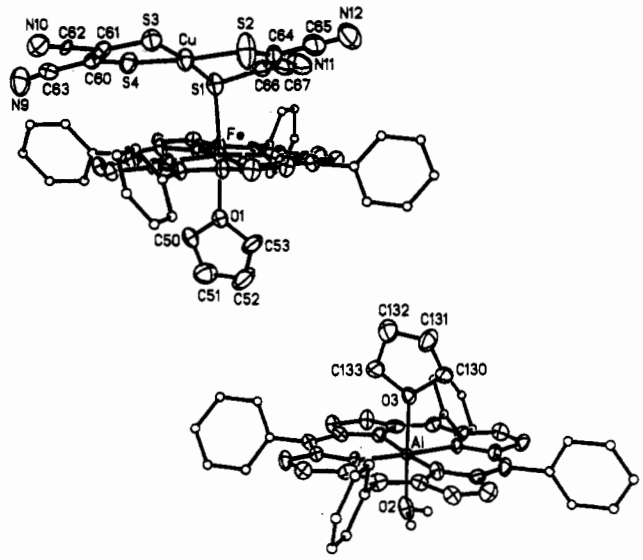

Figure 3. View of **3**. Thermal ellipsoids are drawn at the 50% probability level, carbon atoms of the phenyl rings have been drawn as spheres of arbitrary radius for clarity, and hydrogen atoms, except for those of the H_2O molecule, have been omitted. The numbering schemes for the THF and MNT^{2-} ligands are shown.

Spin-state assignments for the Fe(III) atoms are difficult to infer with confidence from the metric results alone. For intermediate-spin ($S = {}^3/_2$) and quantum-mechanically admixed-spin ($S = {}^3/_2, {}^5/_2$) ferric porphyrin systems, Fe–N_P bond lengths should be short (Fe–N_P = 1.98–2.01 Å) relative to the high-spin ($S = {}^5/_2$) case (Fe–N_P = 2.04–2.09 Å).[35-37] The intermediate-spin or admixed-spin cases should also exhibit long axial bonds relative to the high-spin case, and the Fe atoms should be roughly centered in the porphyrin plane in six-coordinate cases.

In the dinuclear anions of **1–3**, the Fe–N average bond lengths are shorter than would be expected for the $S = {}^5/_2$ case (Fe–N_P = 2.01 (1) Å for **1** at 20 °C, 2.00 (1) Å for **1** at −130 °C, 2.00 (2) Å for **2**, and 2.006 (9) Å for **3**). The Fe–S bond lengths in **1–3** (Fe–S = 2.549 (4) Å for **1** at 20 °C, 2.411 (3) Å for **1** at −130 °C, 2.434 (3) Å for **2**, and 2.444 (3) Å for **3**) are long in comparison to the typical Fe–S bond distances in porphyrin complexes (2.30–2.37 Å).[38] The Fe–O bond lengths in the

(33) Plumlee, K. W.; Hoffman, B. M.; Ibers, J. A.; Soos, Z. G. *J. Chem. Phys.* **1975**, *63*, 1926.
(34) Forrester, J. D.; Zalkin, A.; Templeton, D. H. *Inorg. Chem.* **1964**, *3*, 1507.
(35) (a) Scheidt, W. R.; Reed, C. A. *Chem. Rev.* **1981**, *81*, 543. (b) Scheidt, W. R.; Lee, Y. J. In *Structure and Bonding, Metal Complexes with Tetrapyrrole Ligands 1*; Buchler, J. W., Ed.; Springer-Verlag: Berlin, Germany, 1987; p 1.
(36) (a) Scheidt, W. R.; Geiger, D. K.; Hayers, R. G.; Lang, G. *J. Am. Chem. Soc.* **1983**, *105*, 2625. (b) Scheidt, W. R.; Geiger, D. K.; Lee, Y. J.; Reed, C. A.; Lang, G. *Inorg. Chem.* **1987**, *26*, 1039.
(37) (a) Scheidt, W. R.; Lee, Y. J.; Geiger, D. K.; Taylor, K.; Hatano, K. *J. Am. Chem. Soc.* **1982**, *104*, 3367. (b) Scheidt, W. R.; Lee, Y. J.; Tamai, S.; Hatano, K. *J. Am. Chem. Soc.* **1983**, *105*, 778. (c) Levan, K. R.; Strouse, C. E. *Abstracts of Papers* of the American Crystallographic Association Summer Meeting, Snowmass, CO, Aug 1–5, 1983.
(38) (a) Mashiko, T.; Reed, C. A.; Haller, K. J.; Kastner, M. E.; Scheidt, W. R. *J. Am. Chem. Soc.* **1981**, *103*, 5758. (b) English, D. R.; Hendrickson, D. N.; Suslick, K. S.; Eigenbrot, C. W.; Scheidt, W. R. *J. Am. Chem. Soc.* **1984**, *106*, 7258. (c) Elliott, C. M.; Akabori, K.; Anderson, O. P.; Schauer, C. K.; Hatfield, W. E.; Sczaniecki, P. B.; Mitra, S.; Spartalian, K. *Inorg. Chem.* **1986**, *25*, 1891.

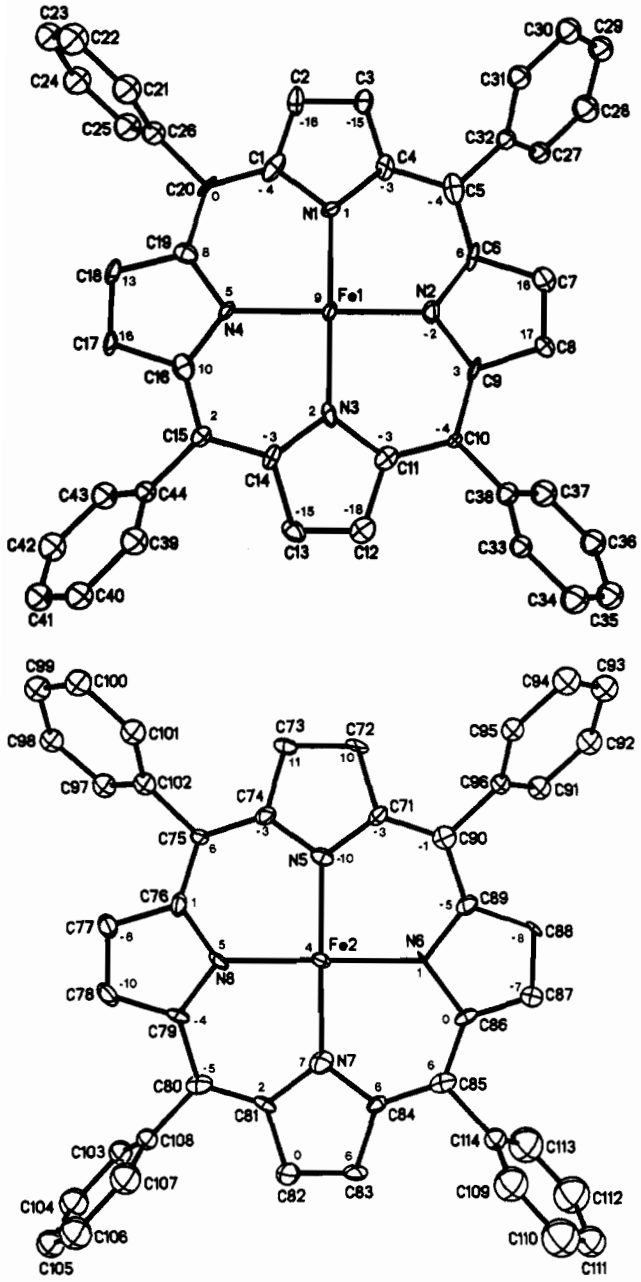

Figure 4. Numbering schemes for the porphyrin units of **1** at −130 °C, where thermal ellipsoids are drawn at the 50% probability level. Also shown are the distances (×10² Å) above and below the best plane through the 24 atoms of the porphyrin core.

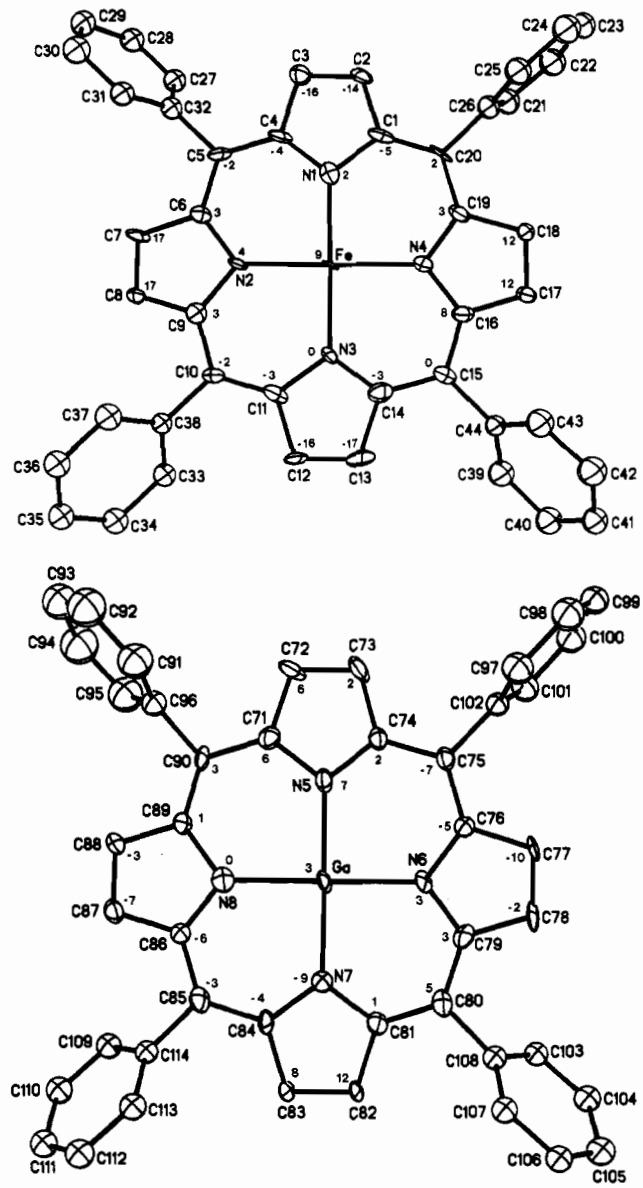

Figure 5. Numbering schemes for the porphyrin units of **2**, where thermal ellipsoids are drawn at the 50% probability level. Also shown are the distances (×10² Å) above and below the best plane through the 24 atoms of the porphyrin core.

dinuclear anions are also long (Fe–O = 2.346 (9) Å for **1** at 20 °C, 2.212 (7) Å for **1** at −130 °C, 2.219 (7) Å for **2**, and 2.255 (7) Å for **3**) when compared to those characteristic of an $S = {}^3/_2$ iron center such as that in $[FeOEP(THF)_2]^+$ (OEP^{2-} = 2,3,7,8,12,13,17,18-octaethylporphyrinate; Fe–O = 2.19 (1) Å).[39] In each case, the Fe atom is displaced from the plane of the porphyrin core toward the bridging sulfur atom ($Fe–Ct_N$ = 0.11 Å for **1** at 20 °C, 0.08 Å for **1** at −130 °C, 0.08 Å for **2**, and 0.09 Å for **3**). These values are larger than expected for six-coordinate intermediate or high-spin iron atoms but are smaller than the values observed for five-coordinate cases ($Fe–Ct_N$ = 0.26–0.28 Å for $S = {}^3/_2, {}^5/_2$ and 0.39–0.54 Å for $S = {}^5/_2$).[35-37] Taken together, the metric parameters suggest considerable $S = {}^3/_2$ character for the Fe atoms of the dinuclear anions in **1–3**.

The spin state of the Fe(III) atom in the cation of **1** is similarly difficult to infer from the metric results. At 20 °C, Fe2–N = 2.03 (2) Å, Fe2–O(av) = 2.20 (3) Å, and $Fe2–Ct_N$ = 0.02 Å (toward O2); at −130 °C, Fe2–N = 2.040 (3) Å, Fe2–O(av) = 2.16 (3) Å, and $Fe2–Ct_N$ = 0.03 Å (toward O2). The Fe–N distances are close to six-coordinate high-spin values. The Fe–O distances are extremely long at 20 °C and significantly shorter at −130 °C. The metric parameters suggest a significant amount of intermediate-spin character for the Fe2 atom at room temperature and an increasing amount of high-spin character with decreasing temperature. The best assignment based on the metric parameters is an admixed-spin state with an increase in the percentage of high-spin character (or possibly even a transition to high-spin character) at lower temperatures.

In **2**, the Ga–N distance of 2.02 (2) Å is within the range found for other Ga(III) porphyrins (2.013–2.034 Å).[40] While the Ga–O(av) distance of 2.13 (3) Å is much longer than the 1.908 (6) Å distance found in $GaOEP(O_3SCF_3)$,[40a] the latter is only five-coordinate and the ligand is negatively charged. The $Ga–Ct_N$ distance of 0.02 Å (Ga(III) displaced toward O2) is much smaller

(39) Masuda, H.; Taga, T.; Osaki, K.; Sugimoto, H.; Yoshida, Z. I.; Ogoshi, H. *Bull. Chem. Soc. Jpn.* **1982**, *55*, 3891.

(40) (a) Boukhris, A.; Lecomte, C.; Coutsolelos, A.; Guilard, R. *J. Organomet. Chem.* **1986**, *303*, 151. (b) Coutsolelos, A.; Guilard, R.; Bayeul, D.; Lecomte, C. *Polyhedron* **1986**, *5*, 1157. (c) Coutsolelos, A.; Guilard, R.; Boukhris, A.; Lecomte, C. *J. Chem. Soc., Dalton Trans.* **1986**, 1779.

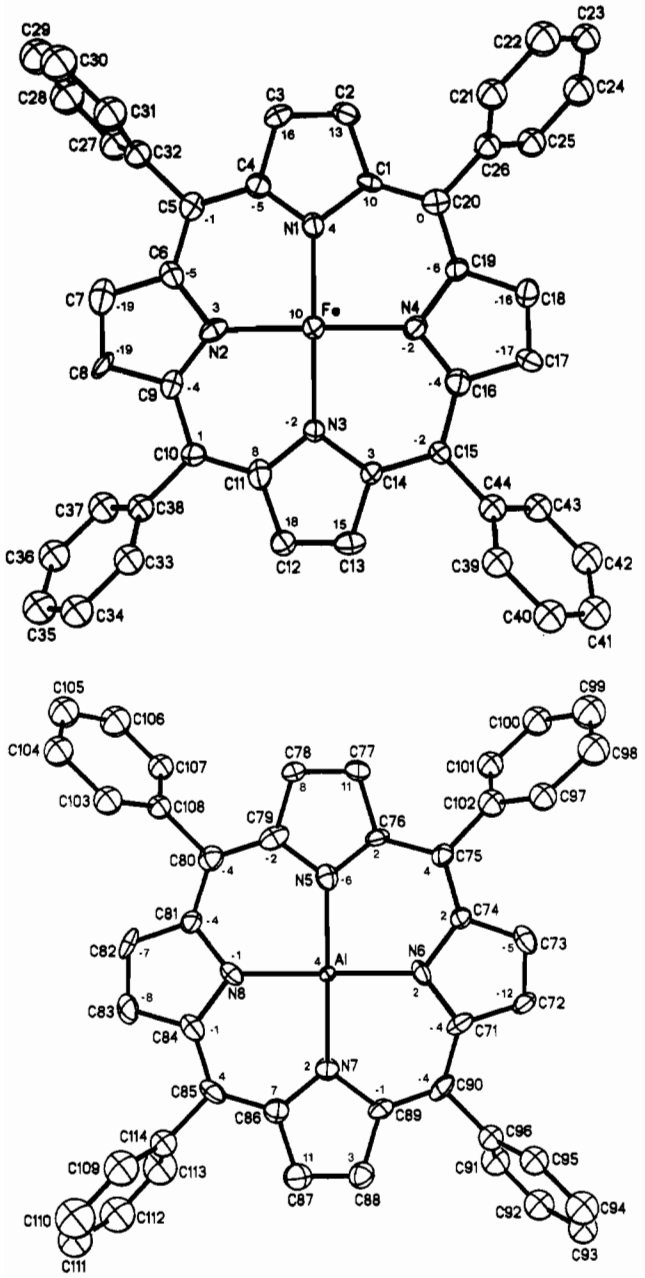

Figure 6. Numbering schemes for the porphyrin units of **3**, where thermal ellipsoids are drawn at the 50% probability level. Also shown are the distances ($\times 10^2$ Å) above and below the best plane through the 24 atoms of the porphyrin core.

than that found in other Ga(III) porphyrin complexes (0.32–0.38 Å),[40] but all other gallium porphyrins that have been structurally characterized are five-coordinate rather than six-coordinate. In the six-coordinate case, the Ga(III) atom would be expected to be roughly centered in the porphyrin plane.

The Al(III) porphyrin cation in **3** is the first such cation to be characterized by X-ray diffraction, although the neutral [Al(OEP)(CH_3)] complex (OEP = 2,3,7,8,12,13,17,18-octaethylporphinate anion) has been structurally characterized.[41] The structural parameters may also be compared to those found for Al(Pc)(Cl)[42a] and $[Al(Pc)]_2O$[42b] (Pc^{2-} = phthalocyaninate). The Al–N distance of 1.998 (6) Å is similar to the values found for the (phthalocyaninato)aluminum(III) complexes (1.98 (1) and 1.98 (3) Å)[42] and slightly shorter than the average Al–N distance in the neutral OEP complex (2.033 (3) Å).[41] The Al–O distances of 1.912 (8) Å (Al–O2) and 2.069 (7) Å (Al–O3) are considerably longer than the value from the μ-oxo–phthalocyaninate complex (1.679 (2) Å),[42b] but again the phthalocyaninate complex is only five-coordinate. As in the Ga(III) case above, the Al(III) atom is roughly centered in the porphyrin plane (Al–Ct_N = 0.05 Å (toward O2)).

The Fe–S bond lengths in **1–3** are similar to those found for the previously studied tetranuclear complexes (Fe–S = 2.44–2.55 Å).[8] These long Fe(III)–S bond lengths must result from the bridging character of the sulfur atom, since a similar ligand in a nonbridging mode (in $(\mu\text{-FNT-}S,S')[Fe(TPP)]_2$, where FNT^{2-} = *trans*-1,2-dicyanoethylenedithiolate)[38c] exhibits "normal" Fe(III)–S bond lengths (2.324 (2) Å). The Fe–S bond lengths approach the value of 2.60 Å suggested by an iron edge EXAFS study of the active site of CcO.[9] The Cu–S(bridging) bond lengths (Cu–S1 = 2.300 (4) Å in **1** at 20 °C, 2.307 (3) Å in **1** at −130 °C, 2.308 (3) Å in **2**, and 2.283 (3) Å in **3**) are close to the Cu–X (X = S or Cl) distance of 2.3 Å seen in copper edge EXAFS studies on CcO depleted of the EPR-detectable copper (Cu_A).[10] The Fe–Cu distances (Fe–Cu = 4.039 (6) Å in **1** at 20 °C, 3.924 (4) Å in **1** at −130 °C, 3.938 (4) Å in **2**, and 3.989 (4) Å in **3**) are distinctly longer than the value of 3.75 Å extracted from Fe and Cu edge EXAFS studies on CcO.[9]

It is important to note the structural similarities between the dinuclear Fe^{III}/Cu^{II} anions in **1–3** (see Table IX). The main structural differences between these compounds reside in the cation, and thus the physical properties of the dinuclear anions are expected to be similar in the three cases.

Magnetic Susceptibility. For compound **3**, calculations of the effective magnetic moment based on experimental values of magnetic susceptibility show that μ_{eff} increases from 2.31 at 4.95 K to 5.01 μ_B at 294.2 K. In the calculation of these results, the experimental susceptibilities (in units of emu mol^{-1}) and the formula $\chi = g^2N_A\mu_B^2[S(S+1)/3kT]$ (with $N_A\mu_B^2/k = 0.375$ in this system of units) were used to calculate the effective magnetic moment per atom, $\mu_{eff} = [3\chi(T)T/0.375]^{1/2}$. The effective spin was then evaluated from the effective magnetic moment by using $\mu_{eff} = g[S(S+1)]^{1/2}$, with the *g*-factor for these qualitative calculations taking the value of 2.0. The above formula is a good approximation only when there is a single pure spin state and the interaction with the external magnetic field is much smaller than kT. It follows from the experimental observations that the effective spin of this system increases with temperature. The large change seen implies that there is a strong admixture of orbital motion to the pure spin state. The effective spin increases, according to the Van Vleck formula, from 0.68 at low temperature to 1.17 at high temperatures.

Thus, the $^6A_1$ singlet is not the ground state of the iron ion, because in this case the expected value for the effective spin should be $^5/_2$. If an isotropic exchange interaction with the copper ion with spin $^1/_2$ is taken into account, the value of the effective spin would lie somewhere between 2 and 3, depending upon the ratio between the exchange parameter and temperature. An exchange interaction alone is unable to explain the observed value of the spin for any value of the exchange parameter even if the ground state had spin $^3/_2$, since it would be impossible to obtain such small values of the effective spin at low temperatures. Thus, there is an additional type of interaction that mixes the orbital motion into the pure spin states and reduces the spin values consistent with the experimental observations. The same consideration holds true for compound **2**.

A least-squares minimization procedure was used to fit the theory to the experimental magnetic susceptibility data, where

(41) Guilard, R.; Zrineh, A.; Tabard, A.; Endo, A.; Han, B. C.; Lecomte, C.; Souhassou, M.; Habbou, A.; Ferhat, M.; Kadish, K. M. *Inorg. Chem.* **1990**, *29*, 4476.
(42) (a) Wynne, K. J. *Inorg. Chem.* **1984**, *23*, 4658. (b) Wynne, K. J. *Inorg. Chem.* **1985**, *24*, 1339.

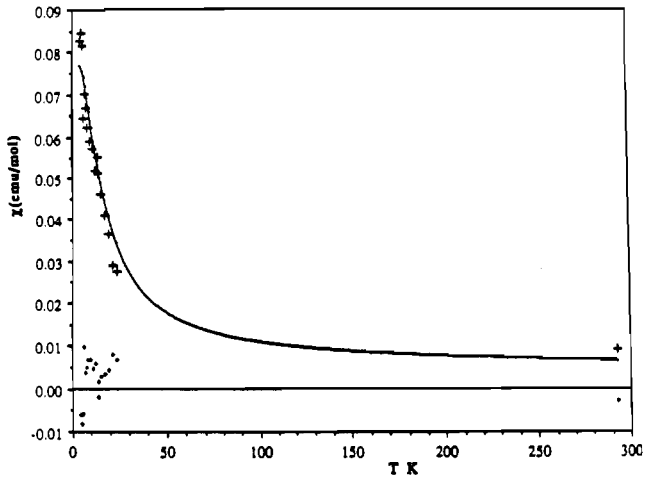

Figure 7. Experimental (crosses) and theoretical (solid line; see eq 7b) magnetic susceptibility (χ) of **2** vs temperature. The difference [χ(theor) − χ(exptl)] at each temperature point is presented in the lower part of the figure.

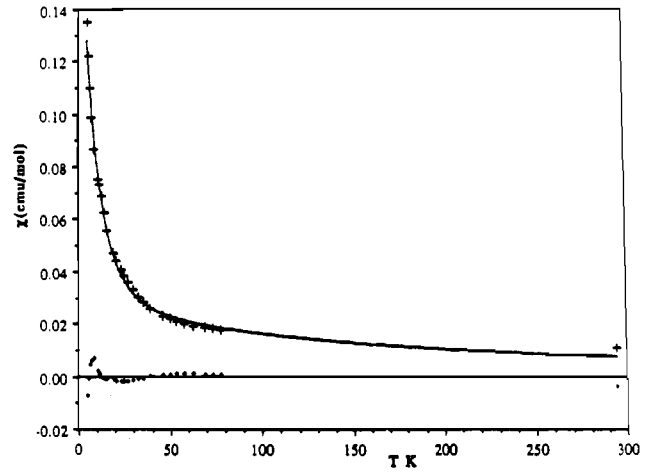

Figure 8. Experimental (crosses) and theoretical (solid line; see eq 7b) magnetic susceptibility (χ) of **3** vs temperature. The difference [χ(theor) − χ(exptl)] at each temperature point is presented in the lower part of the figure.

the *R*-factor was defined as

$$R = \sum_{i=1}^{N} [\chi(T_i) - \bar{\chi}(T_i)]^2 \qquad (11)$$

Here N is the number of temperature points and χ and $\bar{\chi}$ are calculated and experimental magnetic susceptibilities, respectively. For both **2** and **3**, the *R*-factor was minimized over six parameters (see Figures 7 and 8); the best-fit parameters are given in Table X.

Mössbauer Spectra. Figure 9 shows the zero field Mössbauer spectrum of **1** at 77 K. The two Fe(III) sites cannot be resolved by visual inspection or by computer analysis. However, a least-squares fitting procedure to a pair of Lorentzian lines (solid line) yielded line widths of 0.52 mm/s, an artificial broadening attributed to slight differences between the sites. We also note a small amount of impurity in the neighborhood of 0 mm/s that we attribute to high-spin Fe(III). Varying levels of similar impurity spectra were observed in **2** and **3**, as well. These levels did not exceed 5% in any case. The parameters obtained from the fitting procedure are summarized in Table VIII.

Figure 10 shows the Mössbauer spectra of **1** in applied magnetic fields at 4.2 K. The solid lines are the results of the least-squares fits to the spectra based on the two-site model (see above). The spectra in both cases were adequately fit with a single set of parameters for site a. Departures from axial symmetry in the

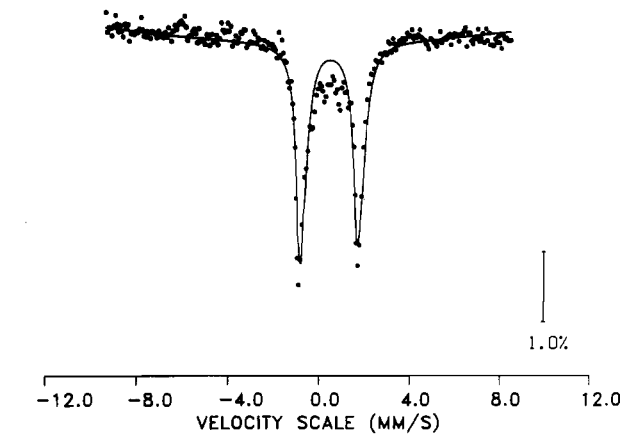

Figure 9. Zero field Mössbauer spectrum of **1** at 77 K. The solid line shows the results of a least-squares calculation (see text for details). The vertical bar indicates 1% absorption.

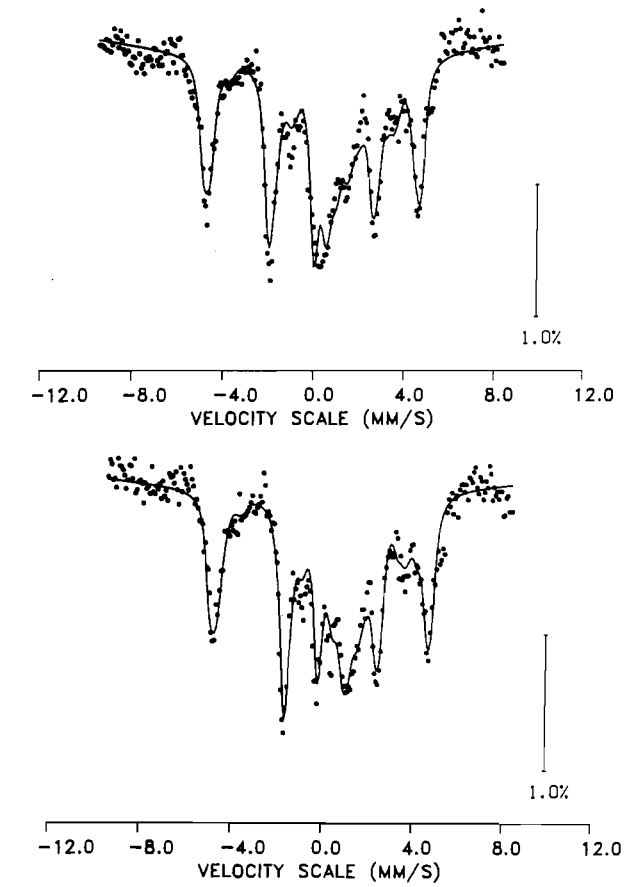

Figure 10. Mössbauer spectra of **1** in 6-T (top) and 8-T (bottom) applied fields at 4.2 K. The solid lines show the results of least-squares calculations (see text for details). Vertical bars indicate 1% absorption.

spin Hamiltonian and the magnetic hyperfine tensor were considered, but they did not improve the fits significantly. Departures from axial symmetry for site b yielded improved fits. Furthermore, the fitted values for the A_{ii} values were different for the two values of applied field. This indicates that the magnetic hyperfine field at the Fe nucleus for site b is not constant as in site a but depends on the magnitude of the applied field.

Both sites show magnetic hyperfine fields that are negative (oppose the applied field), indicating that the magnetic hyperfine interaction is contact-dominated. Thus, the magnetic hyperfine field is expected to be a measure of the local spin density. For a paramagnetic site, we expect the local spin density to be insensitive to the applied field if the latter is large enough (greater than 1 T). For a spin-coupled site, it is possible to have a variation of the local spin density with applied field as the magnetic energy

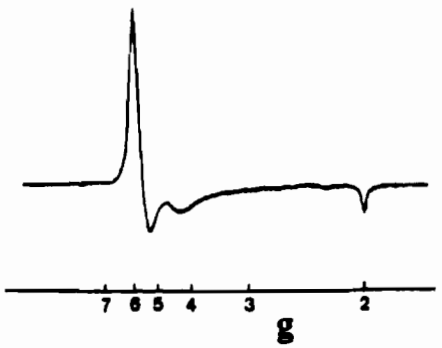

Figure 11. EPR spectrum of **1**. Experimental conditions: 4×10^{-4} M in 1,2-dichlorobenzene glass, 5.7 K, 0.013-mW power, 9.409-GHz microwave frequency, 10-G modulation amplitude, 3.17×10^5 gain.

competes with the exchange interaction. It is reasonable, therefore, to identify site a as the paramagnetic Fe site of the cation and site b as the spin-coupled Fe/Cu site of the dinuclear anion.

EPR Spectra. The frozen-solution X-band EPR spectrum of **1** is shown in Figure 11. The solid-state spectrum at 8.3 K exhibited turning points at the same magnetic fields as shown in Figure 11. There is no feature in the spectrum of **1** which is typical of $[Cu(MNT)_2]^{2-}$.[33,43] The spectrum resembles that of a typical high-spin Fe(III) porphyrin ($g_\perp \sim 6, g_\parallel \sim 2$) with some intermediate-spin character ($g_\perp \sim 4$). Quantitation of the signal by double integration (vs $[Fe(TPP)](O_3SCF_3)$ standard) indicates that ~50% of the total Fe in the sample is observed. This signal is attributed to the Fe(III) atom of the $[Fe(TPP)(THF)_2]^+$ counterion; the sulfur-bridged Fe(III) and Cu(II) atoms of the dinuclear anion are therefore not observed in the EPR spectrum.

The solid-state spectrum of **2** at 5 K exhibits a weak Fe signal (<1%) and a signal typical of $[Cu(MNT)_2]^{2-}$ that varies in intensity between samples, suggesting extraneous $[Cu(MNT)_2]^{2-}$ contamination. The weak Fe signal may be the result of some Ga sites being occupied by Fe (which could also explain the small amount of high-spin impurity seen in the Mössbauer spectrum). The frozen-solution spectrum of **2** contains components similar to those in the spectrum of **1** ($g_\perp \sim 6, g_\perp \sim 4$) as well as a strong component ($g \sim 2$) which is probably due to $[Cu(MNT)_2]^{2-}$. Quantitation of the signal (vs $[Fe(TPP)](O_3SCF_3)$ standard) indicates that ~35% of the total Fe in the sample is observed. The signals observed in the frozen solution spectrum are attributed to fragments resulting from dissociation of the dinuclear anion.

The solid-state EPR spectrum of **3** at 5 K also exhibits a weak Fe signal (again <1%) and no Cu signal. Again, this small Fe signal is probably due to some of the Al sites being occupied by Fe. The frozen-solution EPR spectrum of **3** is very similar to that of **2**. Quantitation of the signals (vs $[Fe(TPP)](O_3SCF_3)$ and $(TBA)_2[Cu(MNT)_2]$ standards) indicates that ~35% of both the Fe(III) and the Cu(II) is again observed. As in the case of **2**, the signals observed in the frozen-solution spectrum are attributed to the results of dissociation of the dinuclear anion.

The EPR results suggest that for **2** and **3** in solution there is some scrambling of the $[Cu(MNT)_2]^{2-}$ anion between the iron and the gallium or aluminum porphyrins. Such scrambling would give rise to Fe(III) and Cu(II) EPR signals, as the metals would no longer be coupled. In **1**, any scrambling would not produce additional EPR signals, since only iron(III) porphyrins are present. Also, this result suggests that no significant amount of free $[Cu(MNT)_2]^{2-}$ is present in solution. The absence of Fe(III) and Cu(II) signals in the solid-state spectra of **2** and **3**, together with the absence of a Cu(II) signal in **1**, supports the assignment of the observed signal for **1** as being that of the $[Fe(TPP)(THF)_2]^+$ cation.

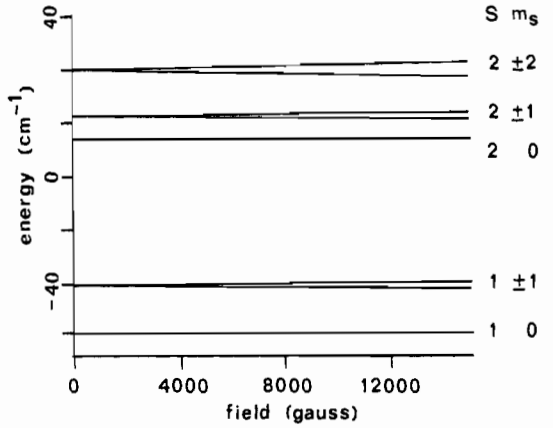

Figure 12. Plot of electron spin energy levels as a function of magnetic field obtained by diagonalization of the energy matrix. The parameters used in the calculation were $2J = -36.0$ cm^{-1}, $r = 4.00$ Å, θ (the angle between the interspin vector and the z-axis of the ZFS) = 30°, $D = 13.28$ cm^{-1}, $g_{Fe} = 1.98$, $g_{Cu} = 2.16$, and $S_{Fe} = {}^3/_2$. The magnetic field was taken to be parallel to the z-axis of the ZFS.

Since the coordination geometries for **2** and **3** are axially symmetric, the following discussion assumes that the magnetic environment is axial and that the zero-field splitting parameter E is approximately zero. In the limit of $J \gg D$, coupling between an $S = {}^3/_2$ center and an $S = {}^1/_2$ center results in $S = 1$ and $S = 2$ states. If the value of D for the $S = {}^3/_2$ center is designated as D_0, the values of D for the $S = 1$ and $S = 2$ states are $1.5D_0$ and $0.5D_0$, respectively.[44] Similarly, coupling between an $S = {}^5/_2$ center and an $S = {}^1/_2$ center results in $S = 2$ and $S = 3$ states with $D = {}^4/_3D_0$ and ${}^2/_3D_0$, respectively. The selection rule for the conventional EPR geometry with the microwave magnetic field perpendicular to the external magnetic field is $\Delta m_s = \pm 1$. For $S = 1$, allowed transitions occur at magnetic fields where the energy separation between the $m_s = 0$ and $m_s = \pm 1$ levels is equal to the EPR quantum (~0.3 cm^{-1} at X-band). As the value of D for a system with integer spin becomes greater than 0.3 cm^{-1}, allowed transitions occur at increasingly high magnetic fields. For integer-spin systems, values of D greater than a few cm^{-1} shift the allowed transitions at X-band beyond the range of magnetic fields generally available. Thus, if the values of J for **2** or **3** were much greater than D, the values of D in Table X and the limiting expressions for D in spin-coupled systems would predict the absence of EPR signals.

Since the values of J for **2** and **3** are of the same order of magnitude as D, the limiting expressions relating D to D_0 are not valid. To check for possible EPR transitions in this regime of $J \sim D > 0.3$ cm^{-1}, the energy levels as a function of magnetic field were calculated by matrix diagonalization. A sample plot using the parameters for **2** with the iron spin state $S = {}^3/_2$ is shown in Figure 12. Inspection of the plot indicates that the energy separation between the $m_s = 0$ and $m_s = \pm 1$ levels exceeds 0.3 cm^{-1} at all accessible magnetic fields. Plots for other orientations of the molecule in the magnetic field and for other combinations of J and D, including values for **3**, also showed energy separations much larger than the X-band EPR quantum. Analogous calculations for $S = {}^5/_2$ iron(III) and values of J and D in the range reported in Table X also showed no accessible allowed transitions. Coupling of Cu(II) to Fe(III) with quantum mechanically mixed $S = {}^3/_2$ and $S = {}^5/_2$ spin states is expected to exhibit energy level separations intermediate between those calculated for $S = {}^3/_2$ and $S = {}^5/_2$ Fe(III). The designations of S and m_s apply, of course, only in the limit of $J \gg D$, and in the intermediate regime represented by these calculations there is substantial mixing of the wave functions.

(43) Snaathorst, D.; Doesburg, H. M.; Perenboom, J. A. A. J.; Keijzers, C. P. *Inorg. Chem.* **1981**, *20*, 2526.

(44) Banci, L.; Bencini, A.; Dei, A.; Gatteschi, D. *Inorg. Chem.* **1981**, *20*, 393.

Since the energy separation between the $S = 1$, $m_s = \pm 1$ levels was equal to 0.3 cm^{-1} at some combinations of molecular orientation and magnetic field, the possibility of a weak transition was explored by calculating the transition probability for the conventional detection geometry. The resonant field was strongly orientation dependent, and the maximum transition probability was less than 1% of that for an allowed transition at the magnetic fields used to obtain the data for **2** and **3**. Thus, the calculations demonstrated that, for a range of values of J and D with $J \sim D > 0.3$ cm^{-1}, EPR spectra would not be observed at X-band for spin-coupled Fe(III)–Cu(II) pairs, including the dinuclear anion in **2** and **3**.

The absence of EPR spectra for **2** and **3** is, therefore, consistent with the parameters obtained from the magnetic susceptibility data. The absence of an X-band EPR signal for the dinuclear anion of **1** suggests that $J \sim D \gg 0.3$ cm^{-1} also holds for **1**. The absence of EPR signals when J and D are greater than the EPR quantum is a general phenomenon and is not limited to the precise values observed for these compounds.

Conclusions

In compounds **1–3**, the same sulfur-bridged Fe(III)/Cu(II) dinuclear anion is associated with slightly different cations. The structural parameters suggest intermediate or admixed spin-state assignments for the iron atom of the dinuclear anion. The parameters derived from the Mössbauer spectra are consistent with intermediate spin-state assignments for the Fe(III) atom of this dinuclear anion. EPR signals are not observed for the sulfur-bridged Fe(III) and Cu(II) atoms of the dinuclear anion, and the exchange coupling constants calculated from the magnetic susceptibility data show that the iron and copper centers of the dinuclear anions are only weakly antiferromagnetically coupled.

These complexes represent, to the best of our knowledge, the first structurally characterized dinuclear Cu(II)/Fe(III) porphyrin complexes in which the two metals are bridged by a single atom and the iron atom is six-coordinate. Furthermore, **2** and **3** represent the first examples of such complexes in which the Cu/Fe pair represent the only paramagnetic centers in the compound. Arguments about the exact nature of the CcO resting state bridge aside, among structurally characterized model systems these complexes represent the closest structural mimics of the resting active site of cytochrome *c* oxidase.

The main experimental evidence in support of the strong coupling model has historically been the absence of an EPR signal and, to a lesser degree, temperature-dependent magnetic susceptibility data. Because of the difficulty of obtaining reliable susceptibility data on large proteins, with their large diamagnetic corrections, the susceptibility data alone do not represent a convincing case for strong antiferromagnetic coupling in the active site. Additionally, mechanisms other than spin coupling can result in lower than expected susceptibilities (e.g., an admixed spin state for the iron). Given the existence of a series of "EPR silent" Fe(III)/Cu(II) systems that are not strongly antiferromagnetically coupled, it would now seem necessary to carefully and critically reexamine the basis for the EPR silence of the active site of the resting form of cytochrome *c* oxidase.

Acknowledgment. C.M.E. and O.P.A. thank the National Institutes of Health (Grant No. GM 30306) for support of this work. The Nicolet R3m diffractometer and associated computing system at Colorado State University were purchased with funds provided by the National Science Foundation (Grant No. CHE 8103011). B.R.S. thanks The Procter and Gamble Co. for support. W.E.H. thanks the National Science Foundation (Grant No. CHE 9111408) for support, and B.R.R. thanks The University of North Carolina for a fellowship. We gratefully acknowledge Dr. Richard B. Frankel's assistance with the collection of the Mössbauer spectra while K.S. was on sabbatical leave at the National Magnet Laboratory, MIT. G.R.E. and S.S.E. thank the National Institutes of Health (Grant No. GM21156) for support. Finally, we wish to thank Prof. Karl M. Kadish for the generous gift of the Ga(TPP)Cl used in this study.

Supplementary Material Available: Tables of crystallographic data, anisotropic thermal parameters, and calculated hydrogen atom positions (14 pages). Ordering information is given on any current masthead page.